Chem Soc Rev

Dynamic Article Links

Cite this: *Chem. Soc. Rev.*, 2012, **41**, 4560–4580

www.rsc.org/csr

CRITICAL REVIEW

Recent advances in large-scale assembly of semiconducting inorganic nanowires and nanofibers for electronics, sensors and photovoltaics

Yun-Ze Long,*[ab] Miao Yu,[c] Bin Sun,[a] Chang-Zhi Gu[d] and Zhiyong Fan[c]

Received 5th December 2011
DOI: 10.1039/c2cs15335a

Semiconducting inorganic nanowires (NWs), nanotubes and nanofibers have been extensively explored in recent years as potential building blocks for nanoscale electronics, optoelectronics, chemical/biological/optical sensing, and energy harvesting, storage and conversion, *etc*. Besides the top-down approaches such as conventional lithography technologies, nanowires are commonly grown by the bottom-up approaches such as solution growth, template-guided synthesis, and vapor–liquid–solid process at a relatively low cost. Superior performance has been demonstrated using nanowires devices. However, most of the nanowire devices are limited to the demonstration of single devices, an initial step toward nanoelectronic circuits, not adequate for production on a large scale at low cost. Controlled and uniform assembly of nanowires with high scalability is still one of the major bottleneck challenges towards the materials and device integration for electronics. In this review, we aim to present recent progress toward nanowire device assembly technologies, including flow-assisted alignment, Langmuir–Blodgett assembly, bubble-blown technique, electric/magnetic- field-directed assembly, contact/roll printing, planar growth, bridging method, and electrospinning, *etc*. And their applications in high-performance, flexible electronics, sensors, photovoltaics, bioelectronic interfaces and nano-resonators are also presented.

[a] *College of Physics Science, Qingdao University, Qingdao 266071, China. E-mail: yunze.long@163.com, qdusun@126.com*
[b] *State Key Laboratory Cultivation Base of New Fiber Materials & Modern Textile, Qingdao University, Qingdao 266071, China*
[c] *Department of Electronic & Computer Engineering, Hong Kong University of Science & Technology (HKUST), Hong Kong SAR, China. E-mail: yumiaonju2006@gmail.com, eezfan@ust.hk*
[d] *Laboratory of Microfabrication, Institute of Physics, Chinese Academy of Sciences, Beijing 100190, China. E-mail: czgu@aphy.iphy.ac.cn*

1. Introduction

In the past 20 years, one-dimensional (1D) carbon nanotubes, semiconducting inorganic nanowires (NWs) and polymer nanofibers have been extensively explored as potential building blocks for nanoscale electronics, optoelectronics, chemical/bio/optical sensors/detectors, and energy harvesting/conversion owing to their relatively high carrier mobility and size-related

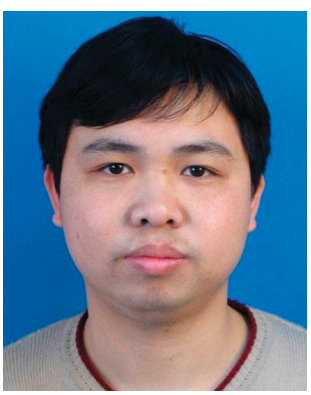

Yun-Ze Long

Yun-Ze Long received his BS degree from University of Science & Technology of China in 2000 and PhD degree from Institute of Physics, Chinese Academy of Sciences in 2005. Then he worked in Institut des Materiaux Jean Rouxel, CNRS, France, as a postdoctoral Fellow. He has been with the Qingdao University since Dec. 2006, where he is currently a full Professor. From 2009 to 2011, he worked as a visiting researcher in the University of Sydney and the HKUST. He has published more than 70 papers, and holds 9 China patents. His research interests focus on 1D functional nanomaterials and devices.

Chang-Zhi Gu

Chang-Zhi Gu received his BS degree from Jilin University in 1986, and then worked as an engineer at Northeast Microelectronics Institute, China. He received his MS and PhD degree from Jilin University in 1991 and 1997, respectively. Then he worked at Fraunhofer Institute for Surface Engineering and Thin Films, Germany and Berlin Free University as a visiting researcher. In 2001, he joined the Institute of Physics (IOP), Chinese Academy of Sciences as a full Professor. Currently he is the director of Laboratory of Microfabrication, IOP. He has published more than 120 papers and holds 20 China patents. His research interests include nanofabrication, nanostructure characterization, and nanodevices.

intriguing physical properties.[1–4] Although patterned nanowires and devices can be fabricated by conventional ultraviolet, e-beam, nanoimprint or other lithography technologies taking advantages of the precision and repeatability of the top-down fabrication,[5] it is becoming obvious that both physical and economic factors of current lithography technologies will limit further advances of the integrated circuit industry. Besides the top-down approaches, nanowires are commonly grown by the bottom-up approaches such as solution growth, vapor–liquid–solid method, and electrochemical deposition into nanoporous templates at a relatively low cost. However, the grown nanowires have random alignment and orientation in most of the cases. In the past decade, a wide range of nanowire-based devices such as field effect transistors, single virus detectors, photo-detectors, and chemical/biological sensors have been demonstrated to show superior performance than their thin-film counterparts.[1–6] Nevertheless, scalable and controlled assembly of nanowires on a variety of rigid or flexible substrates still presents a major challenge toward their potential integration for electronic circuitry, because most of the nanowire devices are limited to the demonstration of single devices, not adequate for production on a large scale at low cost.

Significant efforts have been invested in developing different methods for the assembly of aligned nanowires on various substrates.[7–17] Generally, there are two main strategies for the assembly of nanowire devices: (1) transfer with alignment of pre-grown nanowires onto a desired substrate; (2) direct growth of aligned nanowires or nanofibers onto a desired substrate even at desired locations. In this review article, we summarize recent advances in large-scale nanowire assembly technologies, including flow-assisted alignment, Langmuir–Blodgett technique, contact/roll printing techniques, bridging method, and electrospinning, *etc*. With these approaches, large-scale nanowire array-based thin film transistors have shown operation frequency up to 1.8 GHz.[13] And furthermore, all-nanowire integrated circuits have been successfully demonstrated.[14] These encouraging achievements have shown the promising potential and practical approaches to realize semiconductor nanowire based large-scale high performance electronics, which can enable a whole new generation of flexible electronics for computing, storage, communication, smart sensing and *etc*.

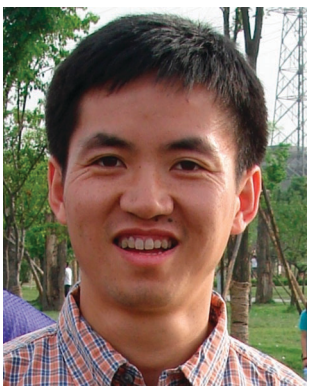

Zhiyong Fan

Zhiyong Fan received his BS and MS degree from Fudan University, China in 1998 and 2001, respectively. He received PhD degree from University of California, Irvine in 2006. From 2007 to 2010, he worked in University of California, Berkeley as a postdoctoral Fellow, with a joint appointment with Lawrence Berkeley National Laboratory. In May 2010, he joined the HKUST as an Assistant Professor. He has published more than 60 papers with more than 2500 citations. He holds 2 China and 1 US patents. His research effort concentrates on engineering novel nanostructures with functional materials for energy conversion, electronics and sensors.

2. Assembly of pre-grown nanowires

At the early stage of nanowire research, nanowire devices are usually made by a "pick and place" method. The typical process is as follows: nanowires are first grown and then harvested and suspended in an organic solvent. Then, nanowires are dispersed onto the desired substrate. Next, an optical or electron-beam lithographic process is applied to pattern metallic contacts to the nanowires. In some cases, the metal microelectrodes are made on the desired substrate before nanowire dispersion, or using a conductive atom-force microscope tip or metal microprobes as electrodes directly.[4] These techniques may be suitable for studying fundamental properties of the nanowires or demonstration of single devices.[1,4] However, they are not appropriate for many device applications or production on a large scale at low cost. The assembly of many individual nanowires over large areas with controlled directions and interspacing is desired for the fabrication of complex circuits of nanowires with logic functions. In the last decade, significant efforts have been invested in developing generic approaches for the assembly of nanowires on various substrates, for instance, flow-assisted alignment, Langmuir–Blodgett, bubble-blown techniques, electric/magnetic-field-directed assembly, and contact/roll printing techniques, *etc*. In this section, we briefly introduce several important approaches.

2.1 Assembly by surface chemical binding or electrostatic interactions

The direct interactions (*e.g*. hydrogen bonding, van der Waals interactions and electrostatic interactions) between the nanowire surfaces and chemically patterned surfaces have been utilized to selectively deposit, assemble and align nanowires without relying on external forces. Many nanostructures such as carbon nanotubes,[18–21] V_2O_5 nanowires,[22] ZnO nanowires,[23] segmented Au/Ni,[24] Au/Ni/Au,[25] Au/Pd/Au[26] nanowires have been assembled on various solid substrates including Si, SiO_2, glass, Au and Al. For example, Kang *et al*.[23] reported two complementary methods for assembly of ZnO nanowires prepared in solution and on solid substrates, respectively. In the solution-phase method, ZnO nanowires were assembled and aligned selectively onto negatively charged surface patterns in solution. While in the solid-phase direct-transfer method, a ZnO nanowire film grown on a solid substrate was placed in close proximity to a molecule-patterned substrate, and ultrasonic vibration was applied so that the nanowires were directly transferred and aligned onto the patterned substrate (Fig. 1a). In addition, a simple method named "surface-programmed assembly" has also been reported by using electrostatic interactions.[22] In this strategy, positively charged surface molecular patterns are utilized to assemble and align negatively charged V_2O_5 nanowires in an aqueous solution over a large surface area ($\sim 1 \times 1$ cm^2), while neutral surface molecular patterns are utilized to avoid any unwanted adsorption of nanowires. Besides, a highly specific and selective assembly of nanowires on pre-patterned Au electrodes using DNA hybridization has been demonstrated recently.[26] In this

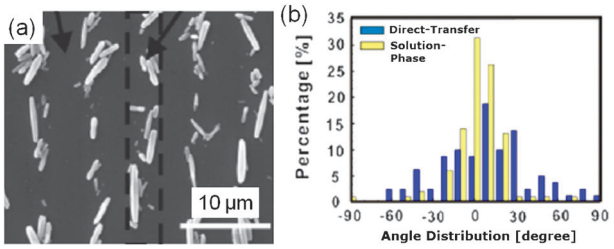

Fig. 1 (a) Scanning electron microscope (SEM) image of ZnO nanowires assembled on a molecule-patterned substrate. (b) Angular distribution of the assembled ZnO nanowires. The angle was measured from the direction of the line patterns shown in (a) (reprinted from ref. 23 Copyright 2008, with permission from IOP Publishing Ltd.).

bio-recognition-directed assembly process, two complementary single-stranded DNAs (*i.e.* DNA_1 and DNA_2) modified with thiol tags are adsorbed on Au electrodes and Au segments of the nanowires, which enable the nanowires to assemble across electrodes.

Surface modification technique can achieve selective deposition (or location control) of nanowires. However, one weakness of this technique is the low percentage of alignment of assembled nanowires,[23] as shown in Fig. 1b. To improve the alignment, one efficient way is to combine this technique with other assembly techniques such as micro-fluidic assembly,[27] contact printing,[28] electric or magnetic field assembly.[24] For example, by combing surface modification with flow assembly, periodically aligned GaP nanowire arrays have been obtained on a SiO_2–Si substrate patterned with NH_2-terminated monolayers in the shape of parallel stripes with a separation of 5, 2 and 0.5 micrometres.[27] In addition, high-density and periodically aligned Ge nanowires have also been obtained on a SiO_2–Si receiver substrate by combing surface chemical modification with contact printing.[28]

2.2 Assembly with microprobes or optical tweezers

Microprobes and optical tweezers (traps) are powerful tools for manipulation of nanoscale materials such as carbon nanotubes[6] and DNA. Recently these techniques have been utilized to assemble nanowires. For instance, cross-nanowire circuits have been reported based on organic single-crystal copper phthalocyanine (CuPc, p-type), copper hexadecafluorophthalocyanine (F_{16}CuPc, n-type) and inorganic Sb-doped tin dioxide (SnO_2:Sb) nanowires.[29] Device fabrication was carried out with microprobes on a micromanipulator probe station. As shown in Fig. 2a and b, first, a layer of poly(methyl methacrylate) was spin-coated onto the substrate as a gate insulator. Second, organic single-crystal nanowires of CuPc or F_{16}CuPc were transferred onto the polymer gate insulator by means of nano-mechanical manipulation. Third, SnO_2 nanowires were transferred to contact the CuPc and F_{16}CuPc nanowires, serving as source and drain electrodes. Based on this technique, versatile functional prototype circuit elements such as inverters, transfer gates, NOR (“Not OR”) gates, and NAND (“Not AND”) gates have been achieved.[29]

In addition, Agarwal *et al.*[30] demonstrated that semiconductor CdS nanowires with cross-sections as small as at least 20 nm can be translated, rotated, cut, fused and organized into nontrivial structures using holographic optical tweezers. Fig. 2c–f shows the detailed process how a rhombus was assembled with CdS

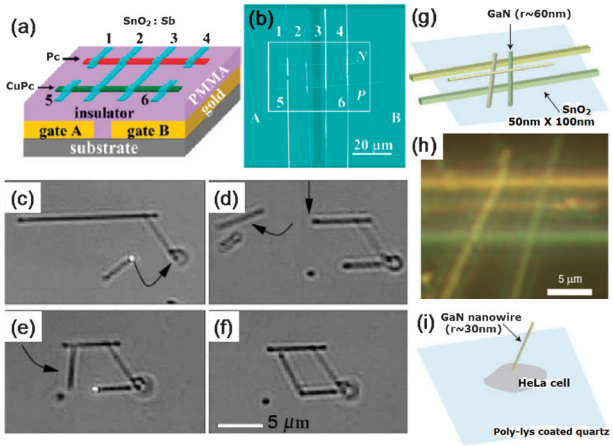

Fig. 2 (a) Schematic illustration and (b) SEM image of cross-nanowire circuits assembled by means of nano-mechanical manipulation (reprinted from ref. 29 Copyright 2009, with permission from WILEY-VCH Verlag GmbH & Co. KGaA). (c–f) Assembly of rhombus with CdS nanowires using holographic optical traps. (c) A nanowire is translated towards an existing structure. (d) The long nanowire is then cut with a pulsed optical scalpel. (e) The resulting nanowire piece then is brought back to the partially completed structure. (f) The rhombus is completed by fusing both ends of the fourth nanowire (reprinted from ref. 30 Copyright 2005, with permission from the Optical Society of America). (g) Schematic and (h) optical dark field image of a 3D nanowire assembly consisting of SnO_2 nanoribbons and GaN nanowires. (i) Schematic of GaN nanowire brought to a human cervical cancer cell by optical trapping (reprinted from ref. 31 Copyright 2006, with permission from Nature Publishing Group).

nanowires by using a holographic optical trapping system. Moreover, Pauzauskie *et al.*[31] showed that an infrared single-beam optical trap can be applied to individually trap, transfer and assemble various semiconductor nanowires (with diameters as small as 20 nm and aspect ratios of more than 100) into arbitrary structures in water (Fig. 2g and h), which may function as active photonic devices. Furthermore, the nanowire structures can also be assembled in physiological environments (Fig. 2i), offering new forms of chemical, mechanical and optical stimulation of living cells. Although microprobe manipulation and optical trapping can control and deposit nanowires precisely, it seems a bit difficult to assemble nanowires on large scales at the present stage.

2.3 Assembly by microfluidic and microchannels

The shear force created by the motion of a fluid against a solid boundary can be used to align nanowires suspended in a solution because the nanowires will reorient to the direction of the fluid flow to minimize the fluid drag forces. Huang *et al.*[27] have developed this technique to align nanowires through confining the fluid flow to a microfluidic channel. In this flow assembly technique (Fig. 3a), a poly(dimethylsiloxane) mold with a microchannel whose width ranging from 50 to 500 μm and length from 6 to 20 mm is brought into contact with a flat substrate. Thus nanowires can be aligned by passing a suspension of nanowires through the microfluidic channel structures. Fig. 3b shows the SEM image of nanowires assembled on SiO_2–Si substrate surfaces within microfluidic flows. And high-performance thin-film transistors using oriented Si nanowire thin films or CdS nanoribbons as semiconducting channels have been demonstrated *via* this method.[9]

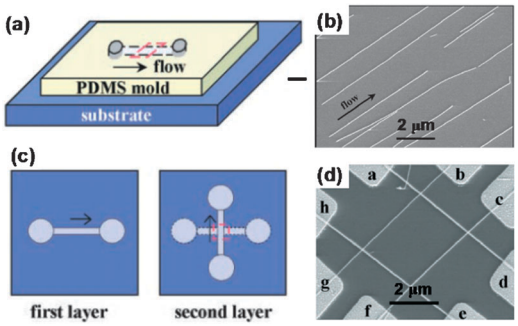

Fig. 3 Fluidic flow-directed assembly of nanowires. (a) Schematic and (b) SEM image of parallel NW arrays obtained by passing a nanowire solution through a channel on a substrate. (c) Schematic and (d) SEM image of a crossed nanowire matrix obtained by orthogonally changing the flow direction in a sequential flow alignment process (reprinted from ref. 27 Copyright 2001, with permission from the American Association for the Advancement of Science).

Furthermore, periodically aligned nanowire arrays have also been obtained by combining the surface modification technique with the flow assembly technique as follows:[27] the substrate is pre-patterned with NH_2-terminated monolayers in the shape of parallel stripes; and then, during the flow assembly process, the nanowires are preferentially attracted to the NH_2-terminated regions of the surface, and the orientation of the nanowires is controlled by the shear force generated from the fluidic flow. In addition, a fluidic flow assembly approach can be also used to organize nanowires into more complex crossed nanowire structures. As shown in Fig. 3c, crossed wire arrays can be obtained by a layer-by-layer deposition process, namely, by alternating the flow in orthogonal directions in a two-step assembly process. The important feature of this layer-by-layer assembly scheme is that each layer is independent of the others and, therefore, a variety of homo- and hetero-junctions can be obtained at the crossed points. By using nanowires with different conduction types (*e.g.* p-Si and n-GaN wires) in each step, the authors have demonstrated logic gates with computational functions from the assembled crossbar nanowire structures (Fig. 3d).[27,32]

Various semiconductor nanowires and nanotubes (*e.g.* GaP, InP, Si, CdS, Ge, single-walled carbon nanotubes, and even duplex DNA) have been assembled by this fluidic alignment approach on a rigid SiO_2–Si substrate and a flexible plastic substrate.[32–34] However, the weakness of this technique is that the area for nanowire alignment is limited by the size of the fluidic microchannels, and it will be more difficult to establish a uniform shear force in a large channel. To improve this approach, Xiong *et al.*[34] recently reported to use a surface-controlled microfluidic method for the fabrication of highly organized single-walled carbon nanotube networks in various dimensions and geometries. As shown in Fig. 4a and b, the SiO_2–Si substrate with lithographically pre-patterned poly(methyl methacrylate) micro-structures was dipped into the carbon nanotube solution along the parallel polymer trench arrays. Subsequently, the substrate was drawn away at a certain rate from the solution. Fig. 4c shows well-aligned carbon nanotubes inside trenches. The highly aligned nanotubes assembled along the geometries of template patterns can be ascribed to nanoscale trenches combined with strong capillary forces and pulling direction

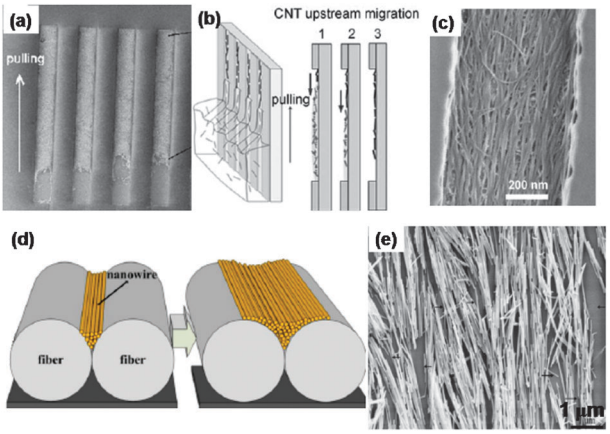

Fig. 4 (a) Microscale template-assisted fluidic assembly by vertically dip coating the poly(methyl methacrylate) template in single-walled carbon nanotubes suspension only once. (b) Schematic illustration of carbon nanotubes migration and assembly in trenches by capillary induced flow. (c) Well-oriented carbon nanotubes assembled in submicrometre trenches (reprinted from ref. 34 Copyright 2007, with permission from WILEY-VCH Verlag GmbH & Co. KGaA). (d) Schematic of more nanowires aligned into the space between nanofibers after several cycles of the evaporation process. (e) SEM image of CdS nanowires aligned on the nanofibers after several dipping–drawing cycles. (Arrows refer to the visible nanofibers) (reprinted from ref. 35 Copyright 2010, with permission from IOP Publishing Ltd.).

(parallel to the trench axis).[34] Here we note that Yan *et al.*[35] also reported a similar template-guided fluidic assembly based on oriented polymer nanofibers. In this case, CdS nanowires dispersed in solution were aligned and selectively deposited at the central space of parallel micro/nano-channels formed by the well-oriented nanofibers as a result of evaporation-induced flow and capillarity (Fig. 4d and e).

2.4 Assembly by the Langmuir–Blodgett technique

Langmuir–Blodgett (LB) technique is usually applied to transfer monolayers of organic materials from a liquid onto a solid substrate to form extremely thin film (LB film) with high degree of structure order. In recent years this technique has been developed for the assembly of nanomaterials, including nanoparticles,[36] nanorods, nanowires, nanotubes, and even two-dimensional nanosheets,[37] which are usually functionalized by surfactants in order to form stable suspensions in the organic solvents.[38] The process of the LB technique for alignment of nanowires is illustrated in Fig. 5a. A nanowire–surfactant monolayer is initially formed on a liquid surface in an LB trough. And the monolayer is then compressed using the barrier under an appropriate level of compression. The nanowires are close-packed as parallel arrays with their longitudinal axes aligned perpendicular to the compression direction to minimize the surface energy of the liquid, and their monolayer is then transferred onto a substrate through vertical-dipping or horizontal-lifting techniques. The spacing between the parallel nanowires can be adjusted by the lifting speed and by the pressure of the compression. For example, Whang *et al.*[39] have successfully transferred Si nanowire monolayers on a 1×3 cm^2 substrate *via* the LB technique, as shown in Fig. 5b and c. The spacing of the transferred nanowires is controlled from micrometre scale to well-ordered and close-packed structures by the compression process.

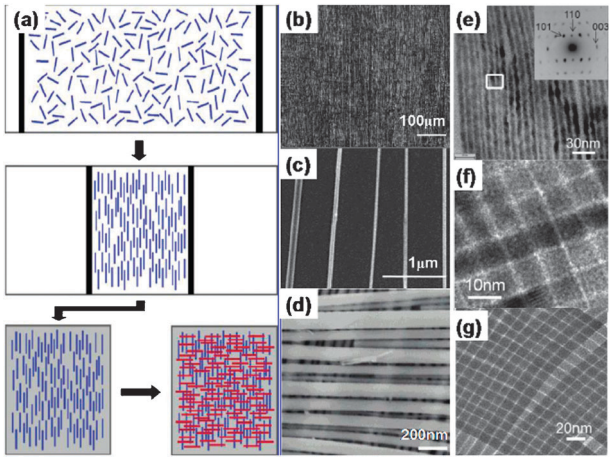

Fig. 5 Alignment of nanowires by an LB technique. (a) Schematic processes of the LB assembly of parallel nanowires and crossed nanowire structures. (b and c) SEM images of an LB assembly of aligned parallel Si nanowires. (d) SEM image of an ultrahigh-density crossed nanowire array (reprinted from ref. 39 Copyright 2003, with permission from the American Chemical Society). (e) Transmission electron microscope (TEM) image of the monolayer assembly of Te nanowires. (f) High resolution TEM image of crossed Te nanowires. (g) TEM image of crossed layers of Ag_2Te nanowires (reprinted from ref. 48 Copyright 2010, with permission from the American Chemical Society).

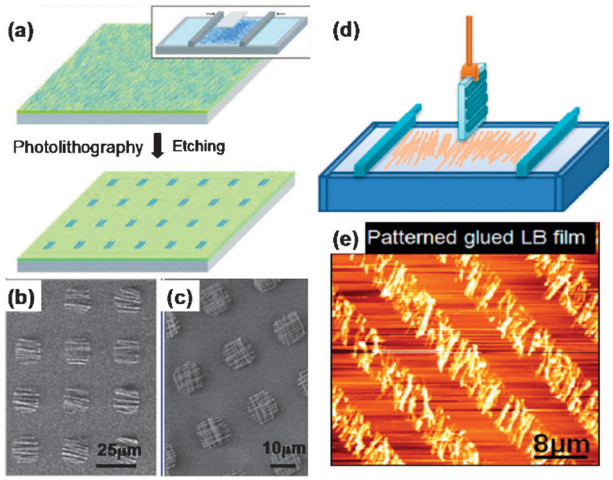

Fig. 6 (a) Schematic illustrating key steps of the interconnection approach, including (top) the deposition of aligned NWs with defined average spacing over the entire substrate, and (bottom) hierarchical patterning to produce fixed size and pitch parallel nanowire arrays (reprinted from ref. 49 Copyright 2004, with permission from the American Chemical Society). (b) SEM image of patterned 10 μm × 10 μm parallel nanowire arrays. (c) SEM image of patterned crossed nanowire arrays (reprinted from ref. 39 Copyright 2003, with permission from the American Chemical Society). (d) Schematic of formation of molecule–V_2O_5 nanowire hybrid film by the gluing LB method on the water surface by compressing the barrier with a surface pressure. (e) Atomic force microscope (AFM) image taken from the hybrid film pattern using a microcontact printing technique combined with the gluing LB method (reprinted from ref. 43 Copyright 2008, with permission from IOP Publishing Ltd.).

Furthermore, hierarchical structures can also be produced by repeating the assembly process after changing the orientation of the substrate (Fig. 5d).[39]

Up to now, various 1D stiff nanostructures, such as Ag NWs,[40] Si NWs,[39] Ge NWs,[41] ZnSe NWs,[42] V_2O_5 NWs,[43] VO_2 NWs,[44] PbS NWs,[45] and $BaCrO_4$ nanorods,[46] as well as single-walled carbon nanotubes[47] have been successfully assembled in large scales by the LB technique. It should be mentioned that Liu *et al.*[48] recently reported that the flexible, ultrathin, and superlong Te nanowires, Ag_2Te nanowires and Pt nanotubes with aspect ratios of at least 10^4 can also be well aligned over a large area by the LB technique to form well-defined periodic mesostructures. Herein, the hydrophilic Te (or Ag_2Te) nanowire–surfactant monolayers can be assembled into aligned nanowire arrays and crossed nanomesh-like mesostructures without any extra hydrophobic pre-treatment or functionalization after synthesis (Fig. 5e–g). In addition, the assembled parallel and crossed nanowire structures can also be patterned into repeating arrays of controlled dimensions and pitch by combining with a conventional lithography technique[39,49] (Fig. 6a–c). Furthermore, Park *et al.*[43] reported on the delicate control of V_2O_5 NWs within the micropatterns transferred *via* the gluing LB technique using a lithographically patterned polydimethylsilicate stamp (Fig. 6d and e). The nanostructures assembled by the LB technique exhibit excellent sensing,[40] electrical[39,49] and photoelectric[48] properties, and have potential applications in ultrasensitive, molecule-specific sensing,[40] and addressable nanoscale devices.[49] The challenges of this technique are the aggregation of NWs in the Langmuir monolayer and the reorientation of NWs during the post processes.

2.5 Assembly within blown bubble films

Recently, Yu *et al.*[50] have demonstrated a general approach for preparing well-aligned and density controlled nanowire and nanotube films over large areas by using bubble expansion of homogeneous nanowire and nanotube suspensions. Fig. 7a shows the basic three steps in this approach: first, preparation of a homogenous, stable, and controlled concentration polymer suspension of nanowires or nanotubes. Second, expansion of the polymer suspension using a circular die to form a bubble at controlled pressure and expansion rate, where stable vertical expansion is achieved using an external vertical force. The nanowires or nanotubes within the film will align along the shear force created by the expansion of the film. At last, transfer of the bubble film to substrates or open frame structures. Fig. 7b gives a photograph of a directed bubble expansion process at the final stage. The ring visible on the top of the bubble moves upwards at a constant speed during expansion. The blown bubble film (bubble diameter of 35 cm; height of 50 cm) has coated the surface of two 150 mm Si wafers. Fig. 7c indicates that the transferred film is uniform over the entire Si wafer, and these Si NWs within the transferred blown bubble film are well aligned along the upward expansion direction (insets, Fig. 7c). The angular deviation of the assembled Si nanowires is less than 10° over the entire 150 mm-diameter wafer. Besides aligned Si nanowire films, CdS nanowires as well as modified single-walled and multi-walled carbon nanotubes have also been successfully transferred to a broad range of rigid or flexible substrates with excellent orientational alignment such as flexible plastic sheets up to 225 × 300 mm^2, highly curved surfaces (Fig. 7d), and suspended across open frames (Fig. 7e), by the blown bubble film approach.

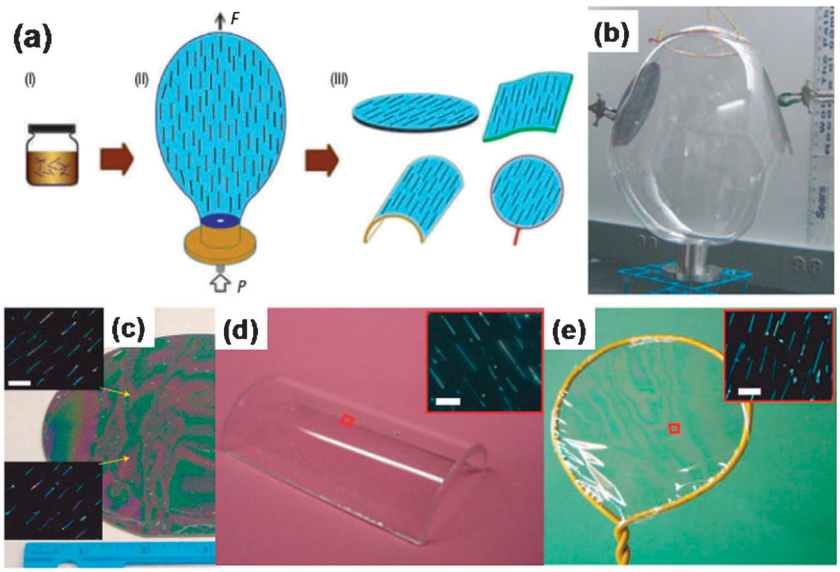

Fig. 7 (a) Illustration of (i) a nanowire polymer suspension, (ii) bubble expansion over a circular die and (iii) films transferred to crystalline wafers, plastics, curved surfaces and open frames. (b) Photograph of a directed bubble expansion process at the final stage. The blown bubble film has coated the surface of two Si wafers. Image of a 0.10 wt% Si nanowire-blown bubble film transferred to (c) a 150 mm Si wafer, (d) a curved surface, and (e) an open frame with a diameter of 6 cm. Insets in (c–e), dark-field optical images showing Si nanowires in the film. The scale bar in (c–e) is 10 μm (reprinted from ref. 50 Copyright 2007, with permission from Nature Publishing Group).

It is noted that the transferred nanowire or nanotube density within the film can be controlled by the concentration of the nanowire/tube in the polymer suspension. In addition, large nanowire field-effect transistor arrays can also show excellent performance when they are fabricated using transferred Si nanowire blown-bubble films on plastic substrates. The weakness of this approach lies in the necessity to embed nanowires/tubes in the bubble films which result in contamination of the nanowires/tubes and possible degradation of their performance. Also, the excess epoxy matrix should be removed using processes such as reactive ion etching before the fabrication of nanodevices.

2.6 Assembly by contact or roll printing

Semiconductor nanowires with desired atomic composition are readily grown by chemical vapor deposition (CVD). The nanowires are typically grown vertically on the substrate, assembling like a forest. The growth substrate can be either planar or cylindrical. For the planar growth substrate, Javey *et al.*[51] and Fan *et al.*[14,52,53] developed a contact printing method for patterned nanowires transferred directly from a nanowire growth substrate to a second device substrate. As illustrated in Fig. 8a, a lithographically patterned receiver substrate is first firmly attached to a bench top, and the nanowire growth substrate is placed upside down on the top of the patterned receiver substrate such that the wires are in contact with the receiver substrate. A gentle pressure is then applied from the top followed by sliding the growth substrate very slowly ($\sim$20 mm min^{-1}). Finally, the growth substrate is removed, and well-aligned nanowire arrays are obtained on the receiver substrate. Here it is noted that surface chemical modification of the receiver substrate can dramatically improve the density of the printed NWs ($\sim$8 NW μm^{-1}).[52] Furthermore, Javey *et al.*[51] have demonstrated that the contact printing technique can be utilized for layer-by-layer assembly of nanowires for 3D multifunctional electronics. As shown in Fig. 8b, to elaborate vertically stacked 3D electronic layers, the nanowire printing and device fabrication steps are iterated multiple times, along with the deposition of an intervening insulation SiO_2 buffer layer.[51]

Particularly, the cylindrical growth substrates used for differential roll printing of nanowires are also reported.[54–56] As shown in Fig. 8c, the differential roll printing approach is based on the growth of crystalline nanowires on a cylindrical substrate (roller) using the vapor–liquid–solid process, and then the directional and aligned transfer of the as-grown nanowires from the donor roller to a receiver substrate by rolling the roller (Fig. 8d). It is found that the nanowire assembly is relatively insensitive to the rolling speed ($\sim$5 mm min^{-1}), but at high velocities ($>$20 mm min^{-1}), non-uniform nanowire printing is attained, arising from the non-conformal contact between the two substrates.[54] The printing outcome, however, highly depends on the roller–receiver substrate pressure, and the optional pressure is $\sim$200 g cm^{-2}. At lower pressures, aligned transfer of nanowires is not observed, and at higher pressures, mechanically induced damage to the nanowires is observed, resulting in the assembly of short wires ($<$1 μm long).

This contact/roll printing method involves the directional sliding of the nanowire growth substrate (either planar or cylindrical) with randomly aligned nanowires on the top of a receiver substrate. During this process, nanowires are effectively combed (aligned) by the directional shear force and are eventually detached from the donor substrate as they are anchored by the van der Waals interactions with the surface of the receiver substrate, resulting in the direct transfer of aligned NWs to the receiver substrate. Since the nanowire printing is performed at ambient temperatures, the process is

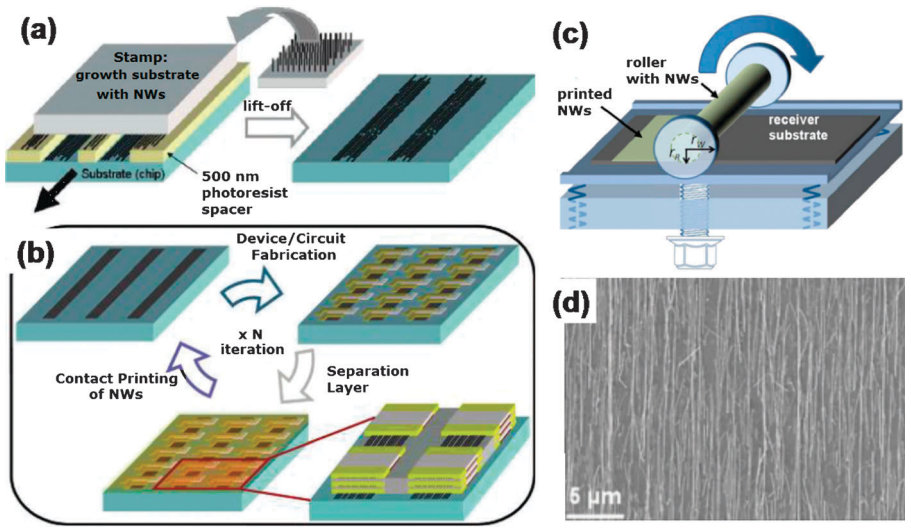

Fig. 8 (a) Contact printing of NWs from a growth substrate to a prepatterned substrate. In general, NWs are grown with random (nonepitaxial) orientation and are well-aligned by shear forces during the printing process. (b) 3D nanowire circuit is fabricated by the iteration of the contact printing, device fabrication, and separation layer deposition steps *N* times (reprinted from ref. 51 Copyright 2007, with permission from the American Chemical Society). (c) Schematic of the differential roll printing. (d) SEM image of Ge NWs printed on a Si–SiO_2 substrate (reprinted from ref. 54 Copyright 2007, with permission from the American Institute of Physics).

highly compatible with a wide range of receiver substrates, such as rigid Si and glass substrates, and mechanically bendable paper and plastic substrates. Furthermore, the process is highly generic for various nanowire materials, including Ge, Si, InAs, CdSe and ZnO.[14,51–56]

Here it is worth mentioning that the transferred semiconductor NWs grown on the donor substrates are usually vertically aligned *via* a CVD process. In fact, for NWs and nanofibers horizontally deposited on donor substrates with random orientation, contact/roll printing is also applicable to obtain aligned nanowire/fiber arrays. For instance, Kim *et al.*[57] proposed a gas-blowing-assisted selective-transfer-printing technique. In their approach, V_2O_5 nanowire sol was used as ink and dropped onto a lithographically pre-patterned polydimethylsiloxane stamp, and then N_2 gas was blown over the stamp to remove excess ink, to dry and align the NWs. At last, the stamp inked with aligned NWs was printed on the positively charged substrate surface. In addition, disordered electrospun nanofibers on Al foil can be transferred onto different receiver substrates such as glass, Si, SiO_2, paper slice, and plastic slice with high alignment by the contact-transfer printing method.[58]

2.7 Assembly by dielectrophoresis or electric fields

Dielectrophoretic assembly technique, namely, electric field-assisted assembly of NWs suspended in a dielectric medium between two electrodes is a promising approach to manipulate NWs due to the ability to position individual NWs precisely on a substrate.[8,10,59–69] The applied electric fields can be used effectively to attract and align NWs normally by the dielectrophoresis forces, which are exerted on the dielectric NWs through the induced dipoles.[60,61] Up to now, various nanostructures, such as Au NWs,[60] Rh NWs,[9] Ag NWs,[65] Si NWs,[9] Se NWs,[65] axially modulated pn Si NWs,[67] InP NWs,[8] ZnO NWs,[62,64] CdSe NWs,[63] as well as polymer nanofibers[68] have been assembled by this approach. Fig. 9a and b show the SEM images of NWs aligned between two parallel electrodes and an array of electrodes, respectively, which demonstrate that virtually all of the NWs aligned in parallel along the electrical field direction, and individual NWs can be positioned at specific locations. In addition, by using layer-by-layer alignment with the electric field applied in orthogonal directions in a two-step assembly, crossed nanowire junctions can be obtained.[8] Wang *et al.*[65] have also demonstrated that flexible, high aspect-ratio selenium NWs can be assembled into macroscopic fibers between electrodes over large distances (> 5 cm; for comparison, the common distances are a few or tens of micrometres).

It should be noted that high-yield single-nanowire integration over centimetre-scale chip areas has been achieved *via* dielectrophoresis combined with fluidic assembly, molecular forces and capillary forces.[10,66] For example, Freer *et al.*[66] refined a fluid flow-assisted dielectrophoresis to place single Si NWs on electrodes and attained 98.5% single nanowire yield on > 16 000 electrode pairs fabricated within an area of 4 cm^2. As shown in Fig. 9c, the fluid flow pushes the NWs to pass the electrodes, whereas the dielectrophoresis forces caused by the applied voltages pull the NWs towards the electrodes. Electrostatic forces attract the NWs towards the electrodes surface and to repel each other to avoid trapping two or more NWs between one electrode pair (which results in a self-limiting behavior). Furthermore, large-area silicon and rhodium nanowire resonator arrays (over 2000 single-nanowire resonators) have also been successfully assembled *via* a refined electric filed-assisted assembly technique.[10] The weakness of the dielectrophoresis approach is the need of prefabricated microelectrode arrays for nanowire assembly and the possible reorientation and aggregation of the NWs upon evaporation of the solvent.

2.8 Assembly by magnetic fields

In addition to electric fields, a magnetic field can also be utilized to direct the alignment of magnetic NWs suspended within a solution.[24,70–75] In order to improve the uniformity of

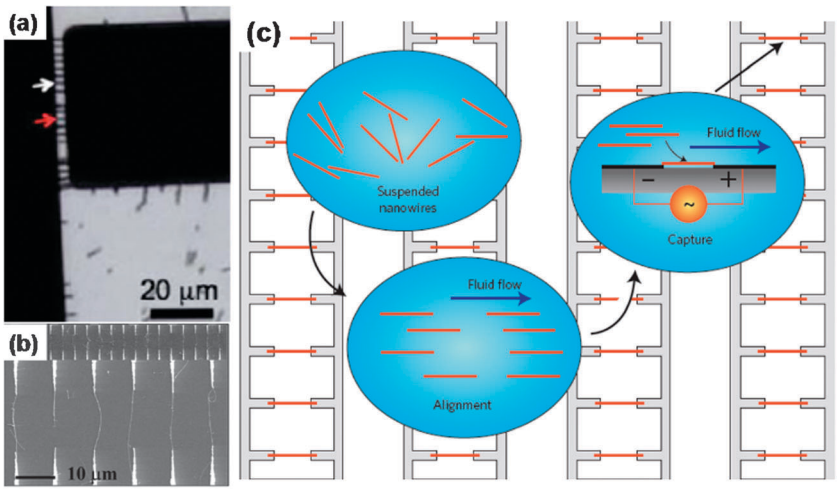

Fig. 9 (a) Image showing assembly of parallel nanowire arrays. The gap between the two electrodes is 3 μm (reprinted from ref. 69 Copyright 2011, with permission from the Royal Society of Chemistry). (b) Spatially positioned parallel array of NWs obtained following electric-field assembly using a bias of 80 V (reprinted from ref. 8 Copyright 2001, with permission from Nature Publishing Group). (c) The foreground depicts a side view of fluid-flow alignment of a colloidal suspension of NWs (shown in red) that are subsequently trapped by dielectrophoretic forces between two neighboring electrodes. If a second nanowire is trapped, it displaces the first NW, which is then carried away by fluid flow. The background portrays a top view of the final array of assembled NWs between electrode pairs (reprinted from ref. 59 Copyright 2010, with permission from Nature Publishing Group).

the assembled NWs and precisely position individual NWs on a substrate, ferromagnetic microelectrodes (microscale or nanoscale magnets) are usually pre-fabricated on the substrates. For example, by using a combination of external magnetic field and local dipolar magnetic field, Liu *et al.*[70] demonstrated that magnetic Ni NWs can be effectively assembled on templates with Co nanomagnet arrays of a ~100% trapping rate under a low external magnetic field (~10 Oe). Moreover, besides parallel nanowire arrays, hierarchical structures such as cross junction and T junction nanowire networks can also be achieved using a sequential magnetic-field alignment technique.[71] It should be noted that nonmagnetic NWs capped with magnetic ends can be assembled using magnetic field.[72,73] For instance, multi-segmented Ni/Au/Ni, Ni/Bi/Ni, and gold–polypyrrole–nickel–gold NWs synthesized by template-directed electrochemical deposition have been successfully assembled by Myung *et al.*[73] Since NW alignment parallel to the applied magnetic field results from the magnetic moment produced in the suspended NWs, the major weakness of this approach is the materials requirement that the NWs must respond to a magnetic field. Here it is noted that Tanase *et al.*[75] demonstrated the possibility of using magnetic NWs in conjunction with patterned micromagnet arrays to control the spatial organization of cells.

3. Assembly by direct growth

The transfer approaches mentioned above can align NWs and control the position to a certain degree, but one disadvantage of these techniques is their need for transfer media such as liquid and sometimes need for surface modification, which may influence the surface cleanness of the NWs and the device performance. In order to reduce or eliminate post-processing of the NWs, one alternative way is to horizontally or vertically integrate NWs into devices on desired locations or substrates by direct growth. In this section, we briefly introduce several direct growth approaches for nanowire device integration, including direct growth of vertical nanowire arrays, planar growth of NWs, bridging method, electrospinning, and template-guided growth, *etc.*

3.1 Direct growth of vertical nanowire arrays

Aligned vertical NWs can be obtained by using either a vapor–liquid–solid method or a vapor–solid method usually, where NWs are grown on the top of a substrate pre-covered by nanosized seeds. The substrate is chosen to have a proper lattice to match with the NWs so that the NWs can be epitaxially grown from the substrate to achieve better alignment, and metal catalyst as Au is sometimes required. For example, Yang *et al.*[76] have synthesized aligned ZnO NWs *via* a vapor–liquid–solid growth mechanism using Au as the solvent. And observation of lasing action in these nanowire arrays indicated that these single-crystalline, well-facetted NWs can function as self-contained optical resonance cavities. In a similar way, Fan *et al.*[77] have demonstrated a method for large-scale fabrication of hexagonally patterned and vertically aligned ZnO NWs. By modifying the electrochemical parameters and growth conditions, the diameter of the nanowires can be varied in the range 30–110 nm. And by using In as a catalyst for growth and simultaneously as a doping source, ordered arrays of n-type ZnO single crystal nanorods have been perpendicularly grown on p-GaN/Al_2O_3 substrates with a vapor phase transport growth method.[78] Besides, Wang *et al.*[79,80] have provided an efficient approach for fabricating highly ordered 1D nanostructures at a wafer scale by combining the laser interference patterning and the hydrothermal method without using microfabrication technology. And according to their experiments, vertically aligned and site controllable ZnO nanowire arrays can be synthesized and replicated *via* a hydrothermal method on general flexible substrates (as shown in Fig. 10).[79]

Gao *et al.*[81] have reported the use of galvanic displacement processes to selectively deposit Au nanoclusters on Si surfaces

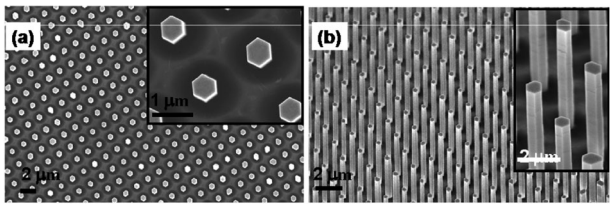

Fig. 10 (a) Top-view and (b) 45°-tilted-view SEM images of vertically aligned ZnO nanowire arrays on a GaN substrate in a large-scale uniform pattern *via* a hetero-epitaxial growth by combining laser interference lithography (reprinted from ref. 79 Copyright 2010, with permission from the American Chemical Society).

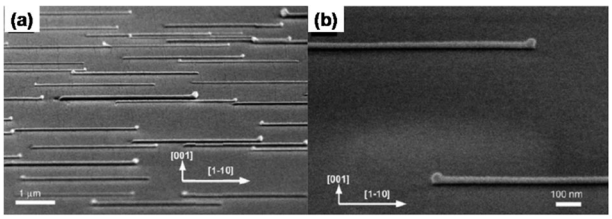

Fig. 11 (a and b) 75°-tilted-view SEM images of well-aligned ⟨110⟩ planar GaAs nanowires grown on a GaAs (100) substrate. Nanowires were grown at 460 °C in (a) and at 475 °C in (b) (reprinted from ref. 90 Copyright 2008, with permission from the American Chemical Society).

for the growth of vertically and laterally aligned Si nanowire arrays. And water-in-oil microemulsions are employed in this process to control the size of the Au clusters, which in turn control the size of the NWs synthesized by the vapor–liquid–solid method. Moreover, Manandhar *et al.*[82] have grown vertical Ge nanowire arrays using chemical recognition and electrophoretic methods, where chemical recognition provides highly reproducible control of the position and number of nanoparticles per pattern element and is shown to be in good agreement with a simple electrostatic model. And vertical transfer of Si nanowire arrays with uniform length onto adhesive substrates was realized by the assistance of creating a horizontal crack formed by adding a water soaking step between consecutive Ag-assisted electroless etching processes of Si.[83] Furthermore, aligned GaAs NWs[84] and even polymer nanowire arrays[85] can also be obtained by vertical growth.

Also, by thermal evaporation of a ZnO:C powder, the effect of the powder source temperature and substrate temperature during the process of ZnO NWs growth has been analyzed.[86] And Lee *et al.*[87] have observed that the NW growth parallel to the local temperature gradient is spontaneous and directional, with a significantly increased growth rate compared to the isothermal growth. Particularly, Wang *et al.*[12,88] have explored the fundamentals of nanowire-based piezotronics and piezo-phototronics.

3.2 Planar growth nanowires

Planar growth nanowires, usually inorganic semiconductor materials, can be obtained by growing nanowires in the plane of the substrate surface under unconventional growth conditions.

Using a phase transport process, Nikoobakht[89] has fabricated well-aligned planar ZnO nanowires on an α-plane sapphire substrate whose surface was pre-patterned with Au nanodroplets, and the growth axis of the planar ZnO nanowires was along the $\pm[1\bar{1}00]$ directions. Fortuna *et al.*[90] obtained controlled growth of planar ⟨110⟩ GaAs nanowires on a GaAs (001) surface using the atmospheric pressure metal organic chemical vapor deposition (MOCVD) and Au catalyst (Fig. 11), and they found that at low growth temperature (<450 °C), GaAs nanowires preferred to grow in the ⟨111⟩ B direction whereas at higher growth temperatures (>450 °C) planar ⟨110⟩ nanowire growth was preferred. TEM manifested that the self-aligned planar ⟨110⟩ NWs are zinc-blende, mostly free of stacking faults, and have an epitaxial relationship with the (001) surface. Furthermore, the n-type planar ⟨110⟩ GaAs NW can be used as the channel material of a metal-semiconductor field effect transistor.[91] Zhang *et al.*[92] have fabricated parallel aligned GaAs nanowires with ⟨110⟩ orientation laterally grown on [311]B substrates *via* the vapor–liquid–solid method, and they demonstrated that the growth is dependent on the polarity of the substrates and the lateral nanowires have to be faceted by facets with low surface energies. And with an In/Ga source mole ratio of 20 : 80, the same team mentioned above has obtained ternary $In_{0.04}Ga_{0.96}As$ nanowires grown on a GaAs (311)B substrate in the Au-particle-catalyzed vapour–liquid–solid method.[93] Herein, the addition of 4% indium changed the cross section of the lateral from the triangular shape of GaAs nanowires to a trapezoidal shape. In addition, Zhang *et al.*[94] have fabricated Mg_2SiO_4 nanowires on Si substrates catalyzed by Au nanoparticles, and the epitaxial growth of the nanowires is confined along the Si ⟨110⟩ directions. Using Ag and Au nanoparticles as catalysts, single-crystalline, well-aligned ZnS nanowire arrays along the [111]B direction are epitaxially grown on GaAs substrates by metal–organic chemical vapor deposition, and the ZnS nanowires undergo a structural transformation from wurtzite to zinc blende with increasing diameter recently.[95]

3.3 Assembly by bridging method

Since keeping the nanowire surface clean is of significant importance for nanowire sensors and detectors, in order to avoid a post-microelectrode-fabrication process, a bridging method has been proposed to grow nanowires from one desired location directly to another desired location, such as between two electrodes. In recent years, this technique has been used to fabricate bridging nanowire devices such as gas sensors, photodetectors, and transistors with Si, GaN, and ZnO.[96–107]

The bridging method which was first demonstrated by Haraguchi *et al.*[96] by growing GaAs nanowires means that the wires can be laterally grown across a trench between two electrode posts which were already etched on a substrate. The schematic diagrams are shown in Fig. 12a. Recently, some achievements have been made in this field. For example, Islam *et al.*[97] fabricated Si NWs between two vertical silicon surfaces by using the metal catalyst—Ti or Au (Fig. 12b). Tabib-Azar *et al.*[98] measured the mechanical properties of this type of Si nanowires, and He and Yang[99] detected the piezoresistance effect of the Si nanowires. The result showed that the nanowires could withstand a maximum bending stress in the range of 210–830 MPa, depending on the nanowire diameter and loading conditions and the longitudinal piezoresistance coefficient along the ⟨111⟩ direction increased with decreasing diameter for p-type Si nanowires. In addition, a series of well-aligned and contact-barrier-free GaN nanobridge devices have been fabricated,[100] the *c*-plane n^+-GaN electrode posts

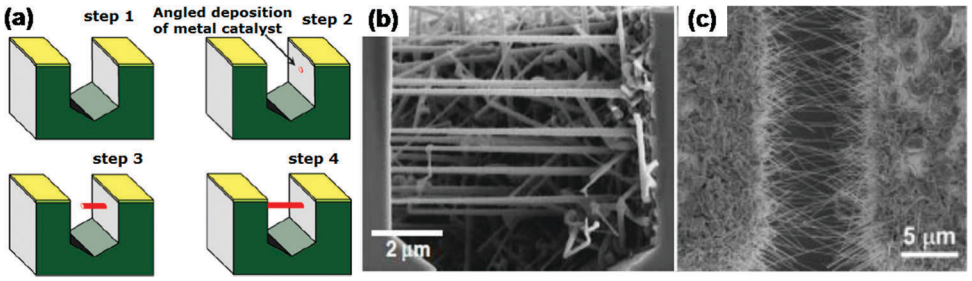

Fig. 12 (a) Schematic diagrams of trench formation (step 1), catalyst deposition (step 2), lateral nanowire growth (step 3), and bridging across trench (step 4). (b) Au-catalyzed, lateral epitaxial nanowire growth across an 8 μm-wide trench, connecting to opposing sidewalls (reprinted from ref. 97 Copyright 2004, with permission from IOP Publishing Ltd.). (c) Top-view SEM image of a GaN nanobridge device focused on the trench with nanowires bridging between two posts (reprinted from ref. 100 Copyright 2008, with permission from WILEY-VCH Verlag GmbH & Co. KGaA).

was along the [100] and [1$\bar{1}$0] sidewalls, and Fig. 12c is the top-view SEM images.

Lee *et al.*[101] had fabricated the ZnO nanobridges without either any metal catalysts or a ZnO seed layer. And horizontal ZnO nanowire arrays on any substrate as long as it is flat, can be grown also. So in this way, the orientation control was achieved using the combined effect from the ZnO seed layer and the catalytically inactive Cr (or Sn) layer for nanowire growth.[102] The growth temperature (<100 °C) is so low that the method can be applied to a wide range of substrates that can be inorganic, organic, single crystal, polycrystalline, or amorphous. Li and coworkers[103] have fabricated the bascule nanobridges which were self-assembled with ZnO nanowires. Here, a high double Schottky barrier was formed at the contact interface of ZnO nanowires self-assembled into bascule nanobridge structures, as shown in Fig. 13a. The difference is shown in Fig. 13c and d where the source material (powder mixture of ZnO and graphite) is increasing from 0.30 g to 0.36 g, and we can see this large amount of source material allows for the growth to continue after the formation of ZnO bascule nanobridges (Fig. 13b). ZnO then nucleates at the nanowire junctions and fuses the nanowires, the contact barriers of these fused nanowires should therefore be reduced when compared with bascule nanobridges.

In addition, materials like InP,[104] Ga_2O_3[105] and Ge[106] nanowires can also be fabricated by the bridging method.

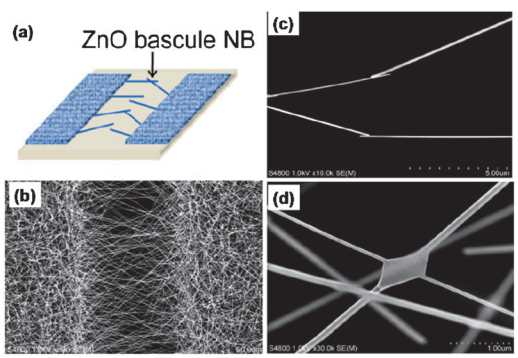

Fig. 13 (a) Schematic of ZnO bascule nanobridges self-assembled in the gap between the ZnO nanowire layers by chemical vapor deposition growth. (b) SEM image of the ZnO bridging nanowires. (c and d) Magnified views of the bridging nanowires in the gap revealing that ZnO grew at the nanowire junctions and fused the nanowires (reprinted from ref. 103 Copyright 2010, with permission from IOP Publishing Ltd.).

In this technique, nanowires can be assembled in a single-step way, so it can minimize the surface contamination because of the electrode posts' pre-fabricated. These nanowire devices can be used as gas sensors, photodetectors, and transistors.[104–106] Particularly, Kim *et al.*[107] demonstrated that this method could be used to directly grow Si nanowire-based AND and OR diode logic gates with excellent rectifying behaviors, and photovoltaic elements in parallel in series, with tunable power output.

3.4 Assembly by electrospinning

Electrospinning is a simple and versatile technique for fabricating uniform ultrafine fibers with diameters ranging from several micrometres down to a few nanometres. During electrospinning, a thin charged jet is formed when the electrostatic force generated by a high operating voltage overcomes the surface tension of the polymer droplet. The jet is accelerated toward the grounded collector and produces ultrathin fibers in the form of nonwoven mats.[108,109] In the past decade, besides polymeric materials,[108–113] inorganic fibers[114–116] also can be fabricated by electrospinning and calcinating. The electrospun fibers have been developed as a good potential candidate in many fields, such as tissue engineering, drug release, nano-sensors, energy applications, biochips, and catalyst supports.[109,115] However, the random orientation of fibrous mats fabricated by the conventional electrospinning may limit the potential applications of electrospun fibers, especially in the fields of electronics, photonics, photovoltaics and actuators which need direct, fast charge transfer or regular, uniform structures. To solve this problem, a variety of strategies have been proposed by many research groups, such as pair electrodes collection, rotating drum or disc collection, auxiliary electric or magnetic electrospinning, double spinning, electroconductive template collection, *etc.*

3.4.1 Rotating collector. The technique of assembling nanofibers by electrospinning with a rotating collector is widely used today.[117] As shown in Fig. 14a, the rotating collector can be a cylinder,[118,119] a wire drum,[120] a wheel/disc[121,122] or a cone.[123] The rotating speed of a mandrel has strong influence on the degree of electrospun fiber alignment. If the rotating speed is too low or too high, the collected fibers are disordered. When the linear speed of the mandrel surface reaches $\sim$2 m s^{-1} (which is the same order of magnitude of the jet velocity), the assembled fibers show high alignment along the axis of rotation.

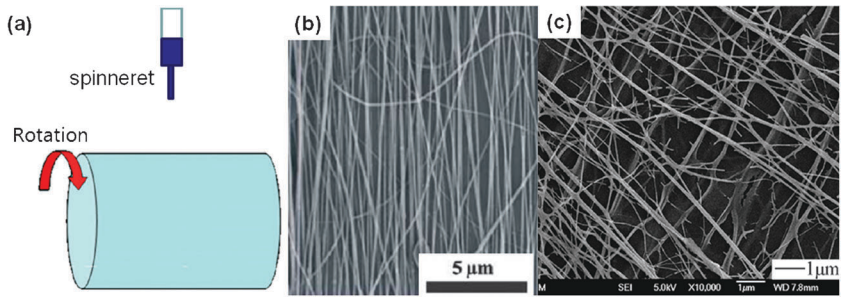

Fig. 14 (a) Schematic illustration of an electrospinning setup using a rotating collector. SEM images of (b) uniaxially aligned TiO_2 nanowires (reprinted from ref. 124 Copyright 2008, with permission from the American Institute of Physics), and (c) cross-aligned ZnO nanofibers fabricated by the rotating cylinder collector (reprinted from ref. 125 Copyright 2010, with permission from the American Chemical Society).

For example, Sundaray *et al.*[118] fabricated continuous aligned polymer fibers when the rotating speed of the cylinder was around 1200–1500 rpm (corresponding to a linear speed of about 2.0–3.0 m s^{-1}). Moreover, fibers were also assembled in criss-cross patterns by spinning in two mutually perpendicular directions on the same substrate. Katta *et al.*[120] employed a Cu wire-framed drum as the collector during the process of electrospinning. As the drum rotates, the charged nanofibers driven by electrostatic interactions are able to stretch and span across the gap between the wires and to form axially aligned arrays over large areas.

This technique was first developed to fabricate aligned polymer fibers. Recently, this technique has been applied to prepare large area of arrayed metal oxide fibers, such as TiO_2[124,126] and ZnO,[125] as shown in Fig. 14b and c. For instance, the aligned ZnO nanofibers can be electrospun on a grounded rotating collector from a precursor gel containing zinc acetate. The spinning time for each layer of ZnO fibers is controlled to be 30 min. The next layer is deposited with an alignment direction perpendicular to that of the previous one. The as-spun ordered ZnO nanofibers are then calcined in oxygen at 450–500 °C by rapid thermal processing to remove organic components and allow the nucleation and growth of ZnO.[125] It is reported that the planar-aligned TiO_2 or ZnO nanofiber architectures (uniaxially aligned nanofibers or multiple layers of cross-aligned nanofiber arrays) can be used in organic–inorganic hybrid solar cells, because the crystalline nanofiber arrays can enhance charge collection and transport rate, as well as facilitate the conjugated polymer infiltration, and thus significantly improve the power conversion efficiency.[124–126] The advantage of this assembly approach is that large area of arrayed fibers can be fabricated. The weakness is that thicker area of arrayed fiber assembly may not be possible.

3.4.2 Gapping method. Uniaxially aligned nanofibers can also be fabricated by introducing an air gap into the conventional collector. In this technique, as shown in Fig. 15a, the collector is divided into two pieces, and by the force originated from the high-voltage splitting electric field, well-aligned nanofibers are stretched across the gap to form a parallel array, which can be conveniently transferred onto the surface of another substrate. The width of the gap between two conductive substrates is varied from hundreds of micrometres to several centimetres. However, it is found that there is a maximum gap size above which the nanofibers are broken (> 1 cm for nanofibers thinner than 150 nm, as an example) that is hypothesized that the nanofibers could not support their own weight beyond a certain length.[127–129] It is believed that the collector materials' relative permittivity could have a profound influence on the deposition behavior of the electrospun nanofibers, and the distance of the collector electrodes' gap are also very important to this technique.[126,127] In this gapping method, the as-spun fibers could be from polymers,[113,127–129] composite materials,[130] semiconducting inorganic materials such as TiO_2,[127] SnO_2,[127] ZnO,[131] Ag-ZnO,[132] $BaTiO_3$,[133] $Li_4Ti_5O_{12}$,[134] boron nitride,[135] and even magnetic materials[136,137] according to their various applications. Fig. 15b–d exhibit the SEM images of uniaxially aligned arrays of ZnO, Sb-doped SnO_2 and $BaTiO_3$ nanofibers assembled by this way. Moreover, the uniaxially aligned arrays of semiconductor nanofibers could be stacked in a layer-by-layer fashion by rotating the collector to generate a 3D net architecture, as shown in Fig. 15e and f. It is found that the aligned fiber arrays show highly anisotropic

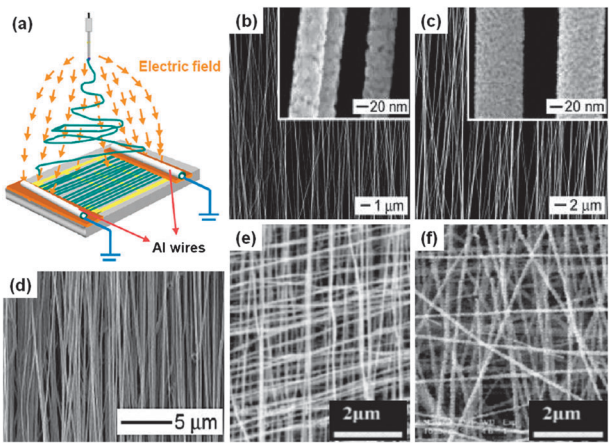

Fig. 15 (a) Schematic illustration of the gapping method setup for electrospinning. The collector contains two conductive Al wires separated by a gap (reprinted from ref. 139 Copyright 2009, with permission from the American Chemical Society). (b–d) SEM images of uniaxially aligned semiconductor nanofibers made of (b) TiO_2, (c) Sb-doped SnO_2 (reprinted from ref. 127 Copyright 2003, with permission from the American Chemical Society), and (d) $BaTiO_3$ (reprinted from ref. 133 Copyright 2006, with permission from Elsevier Ltd). The insets show enlarged SEM images of these semiconductor fibers. (e and f) SEM images of cross-aligned nanofibers network structures made of (e) TiO_2 and (f) $Li_4Ti_5O_{12}$ (reprinted from ref. 134 Copyright 2007, with permission from Elsevier Ltd).

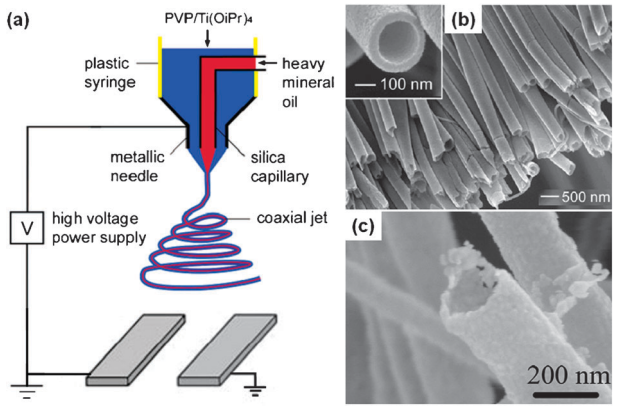

Fig. 16 (a) Schematic illustration of coaxial electrospinning with a pair of parallel electrodes. (b) SEM image of a uniaxially aligned array of hollow TiO_2 fibers which were fabricated by the coaxial electrospinning setup shown in (a). The inset shows an enlarged SEM image of a hollow fiber (reprinted from ref. 138 Copyright 2004, with permission from the American Chemical Society). (c) SEM image of ZnO nanotubes obtained by sputtering ZnO on electrospun polymer nanofiber templates followed by pyrolysis of polymer cores *via* thermal annealing (reprinted from ref. 141 Copyright 2011, with permission from Elsevier Ltd.).

electrical and optical behavior,[127] and have potential applications in optical polarizer,[127] sensitive ultraviolet nanosensors,[131] and 3D batteries.[134]

Besides solid nanofibers, hollow semiconductor fibers with high orientation can also be fabricated by combination of this gapping method with coaxial electrospinning[138] or electrospun polymer nanofiber templates method.[139–141] For example, Li and Xia[138] prepared hollow TiO_2 nanofibers by electrospinning two immiscible liquids (*e.g.* heavy mineral oil and ethanol solution containing poly(vinyl pyrrolidone) and $Ti(OiPr)_4$) through a coaxial, two-capillary spinneret, followed by calcining to selectively remove the cores (Fig. 16a). The uniaxially aligned array of hollow TiO_2 fibers, as shown in Fig. 16b, was collected across an air gap between a pair of split electrodes. In addition, aligned ZnO nanotubes (Fig. 16c) were also prepared by sputtering ZnO onto a sacrificial template made of aligned polymer nanofibers *via* the gapping method, followed by calcining to remove the organic components and crystallize the ZnO overlayer.[139,141] These long hollow nanofibers with well-controlled orientation are particularly attractive for use in fabricating sensitive gas sensors,[139,141] microfluidic devices and optical waveguides. Here, it is noted that although the simple gapping method can be used to fabricate highly aligned nanofibers/tubes which are easily transferable to another substrate, challenges have also been met. For example, it is observed that with the increase of thickness of the electrospun mat, the extent of alignment of the nanofibers decreases due to weakening of the electrostatic force originating from the high-voltage splitting electric field. And it is difficult to mass-produce aligned fibers because most nanofibers are randomly deposited on the electrode surface instead of spanning the gap. So, for practical applications, new improved methods/techniques are still needed in order to mass-prepare ordered ultrathin fibers *via* electrospinning.

3.4.3 Auxiliary electric or magnetic field. Sometimes, the deposition location and degree of alignment of electrospun nanofibers can be controlled by employing an auxiliary electric field or magnetic field. For instance, Deitzel *et al.*[142] have applied a secondary external electric field of the same polarity as the surface charge on the jet by using a series of charged Cu rings as an electrostatic 'lens' element, and when the charged jet passes through this field, it is forced to the center in a manner likely as a stream of water that is poured into a funnel, so it is possible to control or eliminate the bending instability inherent in a conventional electrospinning process. And thus highly aligned nanofibers and pseudowoven mats were produced.[142–144] Cross-aligned nanofiber arrays were also obtained by exploiting an auxiliary electrode subjected to electrical frequencies, which generated crossed arrays on a flat collector.[145] In addition, Wu *et al.*[146] have adopted a modified process to control the width of aligned fiber mats with the help of a rotating drum (as collector) and three parallel auxiliary electrodes. All the electrodes are in the same plane as the top surface of the drum, and when the distance between auxiliary electrodes was decreased, the resulting electrospun fibers were more perpendicular to the axis of the collector and displayed increased fiber distribution density.

Magnetic field can also affect the orientation of electrospun fibers.[147–149] Yang *et al.*[147] have employed a method called magnetic electrospinning to fabricate well-aligned magnetized fiber arrays and multilayer grids by using an auxiliary magnetic field, where the polymer solution is magnetized by the addition of a small amount of magnetic nanoparticles. When the solution is spun into fibers in the presence of a magnetic field generated by two parallel-positioned permanent magnets, the magnetic field stretches the fibers across the gap to form a parallel array as they land on the magnets. In the same year, Ajao *et al.*[148] demonstrated fiber alignment on one face of a box made from Si wafers with a cylindrical magnet inside. Here well-aligned nanofibers were only observed on a particular side (top) of the magnet within the electric-magnetic field while the other sides presented diverse microstructures. This technique is also suitable to build structures with greater complexity than just parallel lines. For example, after collecting the first layer on the substrate, a second layer can be collected by rotating the substrate in a different direction.[147]

3.4.4 Frame collector. In order to obtain an individual nanofiber for the purpose of experimental characterizations, a simply placing frame structure under the spinning jet as a collector is sometimes in use. And this technique for collecting aligned fibers is originated by Huang *et al.*[109] Here, a rectangular frame structure as a collector is placed under the spinning jet, and typical alignments of electrospun fibers have been collected. And it is demonstrated that different frame materials result in different fiber alignments, for example, the Al frame favors better fiber alignments than a wooden frame. In addition, the shape and size of frame rods, the distance between the frame rods, and the inclination angle of a single frame can influence the alignment, too. The same team has also improved this technique by introducing a multi-frame structure, and when it is rotating, the electrospun polymer nanofibers could be deposited on it continuously. Of recent, Tan *et al.*[150] have utilized two parallel strips of a grounded Al frame and a cardboard frame to fabricate polycaprolactone fibers, and the as-spun fiber tested by a nano tensile tester exhibited the characteristic low strength and low modulus but high extensibility at room temperature.

In addition, a Chinese patent[151] demonstrates a novel device with dual rectangular frames as a collector. A large-area nanofiber array (20 × 15 cm^2) with high alignment can be obtained. The frame collector method is similar to a gapping method or a rotating collector in some case, but combines the advantages of these two techniques.

3.4.5 Centrifugal electrospinning. In addition to the rotating collector, highly aligned nanofibers can be produced by a modified electrospinning setup with a rotating spinneret.[152–155] Li *et al.*[152] have invented a novel spinning technique termed double-spinning, as shown in Fig. 17a. In this technique, a lower applied voltage (2.8–3 kV) and the slower rotating speed (390 rpm) are required, which greatly decrease down to one order of magnitude, respectively, in comparison with conventional electrospinning (generally ~10–30 kV) and centrifugal spinning (generally ~3000–8000 rpm). More important, double-spinning has the ability to fabricate an aligned fibrous array. For example, by producing fibers from polystyrene, the team found that more than 95.5% of the fibers are within $\theta = 5^\circ$ (θ is the degree of alignment), and all of the rest are still within $\theta = 10^\circ$ of the desired direction. In other words, the ratio of well aligned fibers can be = 95.5 ± 2.9%, and the SEM image of the parallel aligned fibers is shown in Fig. 17b. Furthermore, more complex structures such as crossbar junctions can also be built by this technique, it can be achieved by a two-step spinning (rotate substrate after the collection of the first layer, and then spin again), as well as what have been mentioned in ref. 30. Fig. 17c–e exhibit the two-layer grids with different rotation angles of 45°, 60°, and 90° generated by the two-step spinning, and the measured angles between fibers in different layers agree well with the rotation angles. Similarly, without the high-voltage electric fields, Badrossamay *et al.*[153] have also generated aligned nanofibers by using high-speed mechanical rotation of solutions through a perforated rotary reservoir, and this structure can be fabricated into an aligned 3D structure or any arbitrary shape by varying the collector geometry.

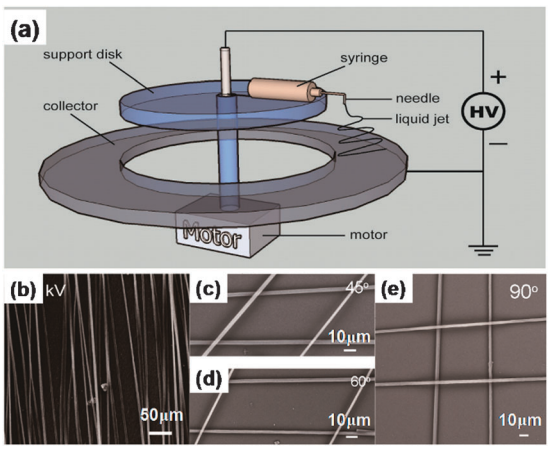

Fig. 17 (a) The schematic illustration of the double-spinning setup. (b) SEM images of the parallel aligned fibers. (c–e) The two-layer grids with different rotation angles of 45°, 60°, and 90°, respectively (reprinted from ref. 152 Copyright 2011, with permission from the Royal Society of Chemistry).

3.4.6 Near-field electrospinning. Near-field electrospinning[156–163] is another powerful way to fabricate orderly nanofibres on flat substrates and realize patterned deposition of nanofibers. In near-field electrospinning, because of the short electrode-to-collector distance (500 μm–10 mm), bending instability and splitting of the charged jet in electrospinning are avoided, so a straight-line jet between the spinneret and the collector can be utilized to direct-write an orderly nanofiber (Fig. 18a). Particularly, by putting the collector on an *X*–*Y* motion stage, the movement of the collector can be controlled in the pre-programmed track *via* a host computer. When the collector speed matches the ejection speed of the jet stream, a mechanical drag force is generated on the suspended nanofiber from the collector and straight-line nanofibers without helical structure can be obtained. And various patterns can be constructed by adjusting the collector speed and track. For example, Chang *et al.*[158] have deposited solid nanofibres with orderly patterns over large areas *via* continuous near-field electrospinning, various complex patterns of polymer fibers have been fabricated (Fig. 18b–e).[158,160] Also, Chang *et al.*[161] have demonstrated piezoelectric poly(vinylidene fluoride) nanogenerators directly written onto a flexible plastic substrate using near-field electrospinning. The energy conversion efficiency is found to be as high as 21.8% with an average of 12.5%, which is much greater than that of typical power generators made from poly(vinylidene fluoride) thin films (0.5–4%). And it could be the basis for an integrated power source in nanodevices and wireless sensors or new self-powered textile by direct-writing nanofibers onto a large area cloth to boost the total power output for portable electronics. Moreover, Rinaldi *et al.*[163] have used the near-field electrospinning to grow well-aligned TiO_2 nanofibers with a diameter of about 200–400 nm on a planar silicon dioxide substrate (Fig. 18f–g). The SEM image shows the presence of microcrystallites, which can increase the gas or tension sensing sensitivity. Compared with other electrospinning techniques, the advantage of this technique is a precise control of the deposition location and pattern of electrospun nanofibers. The weakness is that the assembly efficiency is relatively low.

3.4.7 Conductive template. Chang's group[164,165] obtained electrospun mats with different patterned architectures by collecting fibers with a conductive template as the collector. The template plays an important role in the distribution of electric field, determining the deposition and the arrangement of the fibers in the process of electrospinning. Protrusions and the diameter of the conductive template wires play key roles in the control of the arrangement of the fibers and the architectures of the electrospun mats. Also, the dimensions and spacings of the protrusions as well as the wire spacings in the woven collectors affect the interactions between the fibers and the collector. Another technique called field-enhanced electrospinning has been reported to assemble and pattern as-spun fibers.[166] Polymer fibers were spun on an elastomeric substrate with gold-coated pyramidal protrusions with majority of fibers being deposited at the tips, and nanofiber pattern selectivity is highly dependent on the separation/size ratio of the pyramidal protrusions with a ratio of <1.

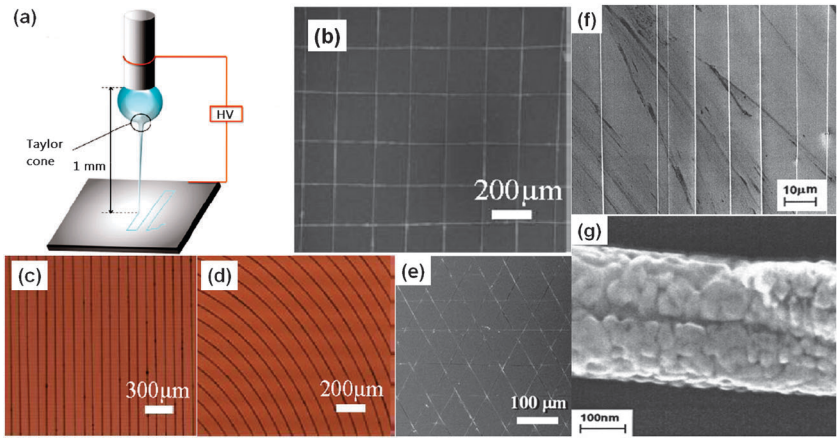

Fig. 18 (a) A schematic of low-voltage near-field electrospinning showing the solution droplet, Taylor cone, and the jet stretched by the electric field and patterned onto a substrate (reprinted from ref. 157 Copyright 2011, with permission from the American Chemical Society). (b) Optical image of a grid pattern with controlled 200 μm spacing. (c) Parallel fibers with controlled 100 μm spacing. (d) Arc pattern with controlled 100 μm spacing (reprinted from ref. 160 Copyright 2010, with permission from Elsevier Ltd.). (e) Optical image of a triangular pattern (reprinted from ref. 158 Copyright 2008, with permission from the American Institute of Physics). (f and g) SEM images of aligned TiO_2 nanofibers at low (f) and high (g) magnifications (reprinted from ref. 163 Copyright 2009, with permission from the American Institute of physics).

3.5 Other approaches

Besides the above-mentioned direct growth techniques, many other approaches have also been reported. For example, electrospinning with a tip collector,[167] template-guided growth,[168,169] colloidal lithography or nanosphere lithography,[170,171] and superlattice nanowire pattern transfer process,[172] *etc.*

The template-guided growth proposed by Martin[168,169] is an effective technique to synthesize arrays of aligned metal, semiconductor, and polymer micro-/nanotubes and wires with controllable length and diameter. Among the various templates, robust porous anodic aluminium oxide templates have been demonstrated to be one of the most promising and most commonly used nanoporous materials. The disadvantage of this method is that a post-synthesis process is needed in order to remove the template.

Colloidal lithography or nanosphere lithography is a very simple, cost-effective, time-effective, and reproductive method to fabricate 1D nanowire and nanocone arrays on many materials in a large scale.[170,171] The general fabrication process is as follows: first, monodisperse colloidal crystals are prepared on the substrate as masks through dip-coating, spin-coating, electrophoretic deposition, or Langmuir–Blodgett assembly, *etc.* and then, the substrates are etched by reactive ion etching. Depending on the conditions of reactive ion etching, either nanowire or nanocone can be obtained.

4. High-performance devices based on assembled nanowires

Large-scale assembled nanowires and nanofibers have many potential applications such as high-performance electronics, optoelectronics/nanophotonics, sensors, nanoresonators, nanogenerators and photovoltaics, particularly in the area of flexible nanodevices. In this section, we review some recent advances in these interesting fields.

4.1 Flexible transistors

The ability to assemble a wide range of nanowire materials on rigid or flexible substrates enables the exploration of a spectrum of device structures such as diodes, transistors, and circuits with desired functionality.[7–9,13,14,32,50–52] For example, printed Si-nanowire arrays were configured as Schottky diodes using asymmetric Pd–Al source-drain contacts on mechanically flexible Kapton substrates, without the use of dopant profiling (such as p–n junctions).[52] The fabricated diodes exhibit highly rectifying behavior, with ~4 orders of magnitude higher forward than reverse currents.

Particularly, Duan *et al.*[9] reported high-performance flexible thin-film transistors based on oriented Si nanowire thin films or CdS nanoribbons. Fan *et al.*[14] also reported that high-electron-mobility (field-effect mobility, $\mu_n > 2000$ cm^2 V^{-1} s^{-1}) InAs nanowires were printed as the channel material for high-performance transistors, capable of delivering high ON currents. More recently, radio frequency response of InAs nanowire array transistors on mechanically flexible polyimide substrates has been demonstrated by Javey *et al.*,[13] as shown in Fig. 19. It is found that the nanowire array transistors exhibit an impressive maximum frequency of oscillation (1.8 GHz) and a cutoff frequency of about 1 GHz. The high-frequency response of the device can be due to the high saturation velocity of electrons in high-mobility InAs nanowires ($\sim 1.3 \times 10^7$ cm s^{-1} at an electric field of 16 kV cm^{-1}). The results present a new platform for flexible, ultrahigh frequency devices with potential applications in high-performance digital and analog circuitry. Furthermore, nanoscale logic gates and computational circuits based on assembled NWs and nanotubes (*e.g.* semiconductor nanowires,[7,32] carbon nanotubes,[6] organic single-crystal nanowires,[29] *etc.*) have also been demonstrated by several groups. For example, inverters, logic OR, AND, and NOR gates were realized using a crossed nanowire p–n diode array.[7,29,32] Importantly, these nanowire logic gates could be interconnected to form an XOR gate and a logic half adder, which was used to carry out digital computations in a way similar to conventional electronics.[32]

4.2 Sensors and detectors

The assembled semiconductive nanowires have also been explored as gas and optical sensors and detectors. For example,

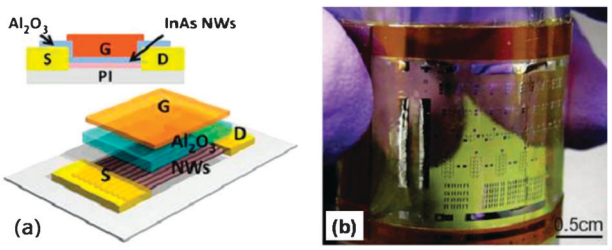

Fig. 19 Schematic and optical images of a printed InAs nanowire array FET fabricated on a flexible polyimide (PI) substrate for GHz operation. (a) Schematic illustration of the nanowire parallel array FET, illustrating the various layers of the device. The cross-sectional image is shown on the top. (b) Photograph image of the fabricated nanowire device array on a bendable polyimide substrate (reprinted from ref. 13 Copyright 2010, with permission from the American Chemical Society).

p-type Si-nanowire arrays were configured as H_2 sensors.[173] To enhance sensitivity to H_2, a 2 nm-thick Pd film was deposited on the printed nanowire array, resulting in the formation of Pd nanoclusters on the nanowire surfaces. It is found that the conductance of the Si-nanowire array shows a strong dependence on the H_2 exposure, even at relatively low concentrations (250 ppm). Li *et al.*[105] also reported the assembly of β-Ga_2O_3 nanowires into high-performance solar-blind (ultraviolet C, 100–280 nm) photodetectors by the bridging method. The device has a high 250-to-280 nm rejection ratio of $\sim 2 \times 10^3$, low photocurrent fluctuation ($<3\%$), and a fast decay time ($\ll 20$ ms).

In addition, printed CdSe-nanowire arrays were used for optical sensing.[174] Importantly, the nanowire sensors and transistors can be assembled to enable on-chip optical sensing and signal amplification.[14,174] Fig. 20a shows the schematic and circuit diagram of an all-nanowire photodetector based on ordered arrays of Ge–Si and CdSe nanowires. Each individual circuit consists of three active device elements: an optical nanosensor based on either a single or parallel array of CdSe nanowires; a high-resistance field-effect transistor based on parallel arrays of 1–5 Ge–Si core–shell nanowires, and a low-resistance buffer field-effect transistor with the channel consisting of parallel arrays of $\sim$2000 Ge–Si nanowires. Furthermore, large-scale heterogeneous integration of parallel-array nanowire circuits was also fabricated on a chip. As shown in Fig. 20b and c, each circuit element in the array operates as a single pixel. To demonstrate the image-sensing functionality of the circuit array, a halogen light source was focused and projected onto the center of the matrix (Fig. 20c), and the photoresponse of each individual circuit element was characterized. The measured intensity level of each circuit was incorporated into a two-dimensional contour plot to create a contrast map (Fig. 20d). This work represents an important advance toward large-scale, heterogeneous integration of nanowire arrays for imaging sensor applications.

Artificial electronic skin (e-skin) that can detect the environment through touch is of profound interest for robotic and prosthetic applications. Recently, nanowire active-matrix circuitry for low-voltage macroscale artificial skin has been demonstrated by Javey and co-researchers.[11] Fig. 21a shows the process scheme for the electronic skin device with an integrated nanowire active-matrix backplane (Fig. 21b).

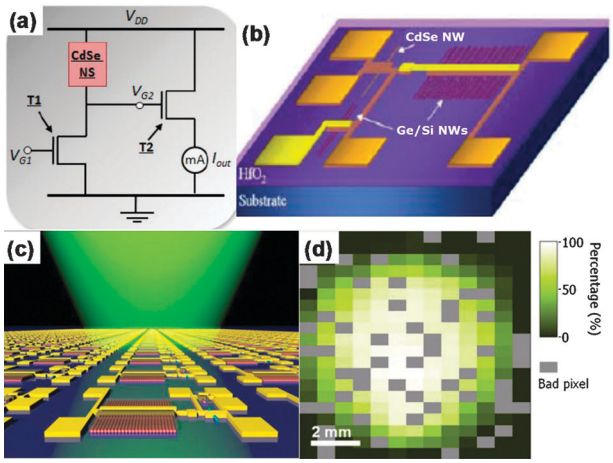

Fig. 20 (a) Diagram of a proof-of-concept nanowire photosensor circuitry, consisting of a CdSe-nanowire light sensor (NS), an impedance-matching nanowire transistor (T1), and a buffer transistor (T2). A light signal is detected by the CdSe nanosensor and the current output signal is then amplified by the two transistors. (b) Schematic of the all-nanowire optical sensor circuit based on ordered arrays of Ge–Si and CdSe nanowires (reprinted from ref. 174 Copyright 2008, with permission from the National Academy of Sciences of the U.S.A). (c) A perspective picture showing the imaging function of the circuit array. (d) 2D circular-light intensity map imaged by the all-nanowire sensor arrays, demonstrating a proof-of-concept image sensing (reprinted from ref. 14 Copyright 2009, with permission from WILEY-VCH Verlag GmbH & Co. KGaA).

Optical images of a fully fabricated electronic skin, consisting of a 19 × 18 pixel matrix with an active area of 7 × 7 cm^2, are shown in Fig. 21c. The structure can easily be bent or rolled to a small radius of curvature. To demonstrate the functionality of the integrated e-skin, a piece of poly(dimethylsiloxane) (PDMS) moulded as the letter '*C*' with an area of $\sim$3 cm^2 is placed on top of the sensor array, followed by the application of a normal pressure of $\sim$15 kPa (Fig. 21d). The elastic poly(dimethylsiloxane) mould enables the uniform distribution of the pressure over an area corresponding to that of the '*C*'. The output conductance for each individual pixel is measured, and plotted as a two-dimensional intensity plot. As depicted in Fig. 21e, the applied pressure profile can be spatially resolved by the integrated nanowire electronic-skin. The pixel resolution used in this work was set to $\sim$2.5 mm to enable a manageable number of pixels without the need to implement system integration for the signal readout. The artificial electronic skin demonstrated here presents one example of the large-scale fabrication of low-cost nanowire sensor circuitry. The ability to controllably achieve functional electronics on truly macroscales using printed nanowire arrays presents a feasible route towards their implementation for practical applications.

4.3 Solar cells and nanogenerators

Assembled semiconducting nanowire and nanofiber arrays have also been utilized to harvest solar energy[124–126,171,175–178] and mechanical energy[53] in recent years. For instance, solar cells based on a dense array of oriented, crystalline ZnO, TiO_2, Si, CdS/CdTe nanowires have been reported by

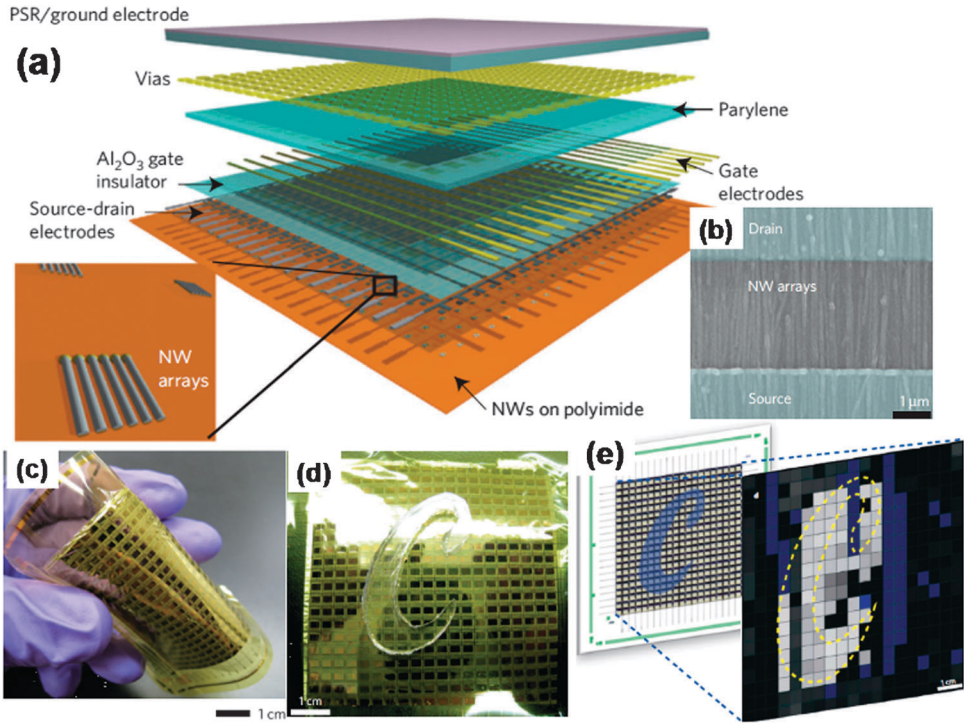

Fig. 21 (a) Schematic of the passive and active layers of nanowire e-skin. (b) SEM image of a nanowire-array field-effect transistor, showing the high degree of nanowire alignment and uniformity achieved by the contact printing. (c) Optical photographs of a fully fabricated e-skin device (7×7 cm^2 with a 19×18 pixel array) under bending. (d) Photograph of a fabricated e-skin with a poly(dimethylsiloxane) mould in the shape of '*C*' placed on the top for applying pressure and subsequent imaging. (e) Design layout of the sensor device (left), and the corresponding two-dimensional intensity profile obtained from experimental mapping of the pixel signals (right). The character '*C*', corresponding to the applied pressure profile, can be readily imaged by the e-skin (reprinted from ref. 11 Copyright 2010, with permission from Nature Publishing Group).

several research groups.[171,175–178] A pioneering work was done by Law *et al.*[175] in 2005. In this work, vertical arrays of ZnO nanowires were grown on F:SnO_2 conductive glass (FTO) substrates (Fig. 22a and b). The electron diffusivity within the wires was estimated to be between 0.05 and 0.5 cm^2 s^{-1}, much higher than that estimated for typically used ZnO nanoparticle films. As shown in Fig. 22c, photovoltaic measurements showed device characteristics of a short circuit current 5.3–5.85 mA cm^{-2}, open circuit voltage 0.61–0.71 V, fill factor 0.36–0.38 and the resulting efficiency 1.2–1.5%. The highest external quantum efficiency of the cell measured was 40% at 515 nm wavelength. Besides vertical nanowire structures (Fig. 22a), planar structures based on assembled nanowires and nanofibers have also been demonstrated. As shown in Fig. 22d and e, Shim *et al.*[124] and Yan *et al.*[125,126] reported hybrid solar cells based on ordered electrospun ZnO or TiO_2 nanofiber arrays with conjugated polymers. It was found that the resultant cells with cross-aligned fibers showed much larger photoinduced current and higher power conversion efficiencies than those with randomly collected nanofibers (Fig. 22f).

In addition, Zhu *et al.*[53] reported a flexible high-output nanogenerator based on lateral ZnO nanowire arrays. Vertically aligned ZnO nanowires on Si substrates were synthesized using a physical deposition method, and then transferred to a flexible receiving substrate to form horizontally aligned arrays. Parallel strip type electrodes were deposited to connect all of the nanowires together (Fig. 23a). As shown in Fig. 23b–d, it was found that the electrical output of the nanogenerator reached a peak voltage of 2.03 V and current of 107 nA with a peak power density of $\sim$11 mW cm^{-3}, which is 12–22 times of that from lead zirconate titanate (PZT)-based cantilever energy harvester. The effective energy generation efficiency was about 4.6%. The electric energy generated by the nanogenerator was effectively stored by capacitors and used to light up a commercial light-emitting diode (LED), which is a landmark progress toward building self-powered devices by harvesting energy from the environment. Furthermore, by optimizing the density of the nanowires on the substrate and with the use of multilayer integration, a peak output power density of $\sim$0.44 mW cm^{-2} and a volume density of 1.1 W cm^{-3} have been achieved.[53]

4.4 Multicolor nano-light-emitting diodes

In addition to a variety of nanoscale electronic device concepts, including crossed nanowire p–n diode, crossed nanowire field-effect transistors, and integrated logic gates and computational circuits, a wide range of photonic and optoelectronics devices such as multicolor light-emitting diode (LED) arrays have also been first demonstrated by Lieber's group.[8,32,179] These diodes can be constructed from crossed junctions of n- and p-type nanowires for differently doped nanowires of the same material such as p-InP/n-InP,[8] or combinations of indirect bandgap p-Si nanowires with inefficient light emission and a broad range of direct bandgap n-type nanowires such as GaN, CdS, $CdS_{0.5}Se_{0.5}$, CdSe, and InP with efficient light emission.[32,179] As shown in Fig. 24a, when the applied forward

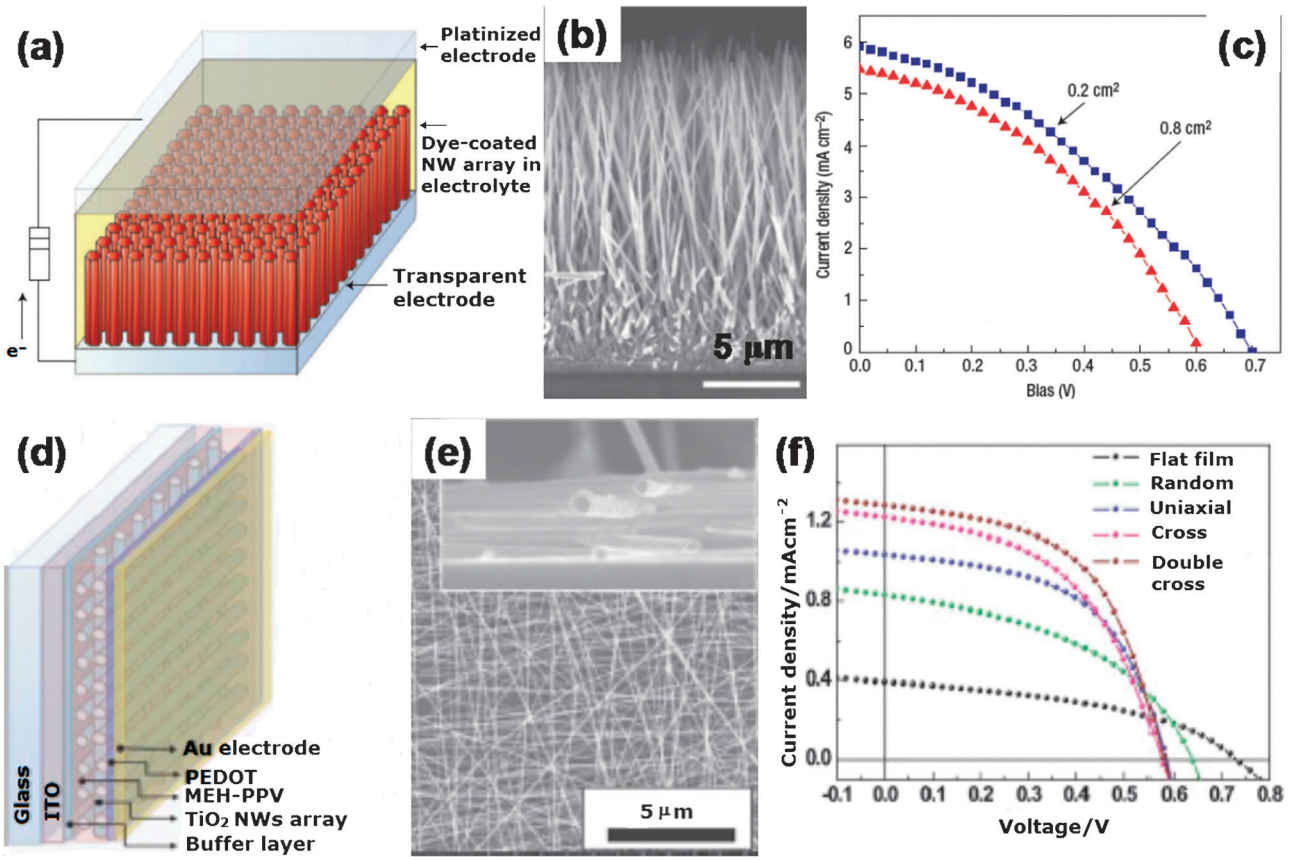

Fig. 22 (a) Schematic diagram of the nanowire dye-sensitized cell based on a ZnO wire array. (b) Typical cross-sectional SEM image of a cleaved ZnO nanowire array on a substrate. (c) Current–voltage curves for two cells with active areas of 0.2 and 0.8 cm^2 (reprinted from ref. 175 Copyright 2005, with permission from Nature Publishing Group). (d) Schematic illustration of hybrid solar cells introduced with aligned TiO_2 nanofibers. (e) SEM image of cross-aligned TiO_2 nanofibers. The inset shows the cross-sectional image. (f) The current–voltage curves for the hybrid solar cells employing the planar-patterned nanofiber electrodes (reprinted from ref. 124 Copyright 2008, with permission from the American Institute of Physics).

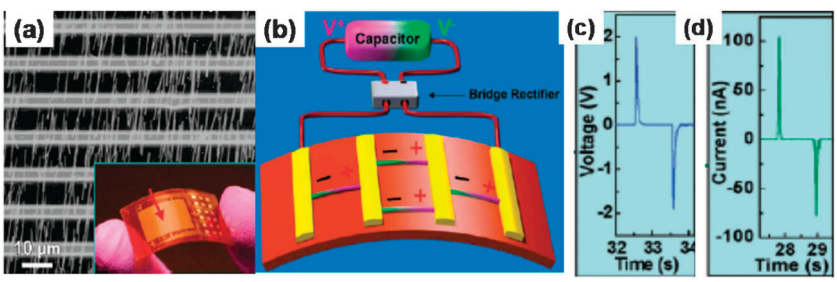

Fig. 23 (a) SEM image of ZnO nanowire arrays bonded by Au electrodes. Inset: demonstration of an as-fabricated flexible high-output nanogenerator. (b) Demonstration of the output scaling-up when mechanical deformation is induced, where the "±" signs indicate the polarity of the local piezoelectric potential created in the nanowires. (c) Open circuit voltage and (d) short circuit current measurements of the high-output nanogenerator (reprinted from ref. 53 Copyright 2010, with permission from the American Chemical Society).

bias voltage exceeds the bandgap, the crossed nanowire heterostructures will emit light characteristic of the n-type nanowire element. The indirect-gap p-Si nanowire is a passive optical component and used for its well-defined electronic properties. Since the emission wavelength depends on the n-type nanowires used, therefore a series of different junctions creates multicolor emission, when various n-type nanowire devices simultaneously addressed by one p-type Si nanowire. Fig. 24b shows a schematic and corresponding SEM image of a tricolor nano-LED array consisting of n-type GaN, CdS, and CdSe nanowires crossing a single p-type Si nanowire, which was fabricated by using a silicon-on-insulator substrate to etch p-Si nanowire assembly and fluid-based alignment technique. Normalized emission spectra demonstrate three spatially and spectrally distinct peaks with maxima at 365, 510, and 690 nm (Fig. 24c) consistent with band-edge emission from GaN, CdS, and CdSe, respectively. In addition, the crossed-nanowire LED devices can also be deposited on flexible polymer substrates.[180]

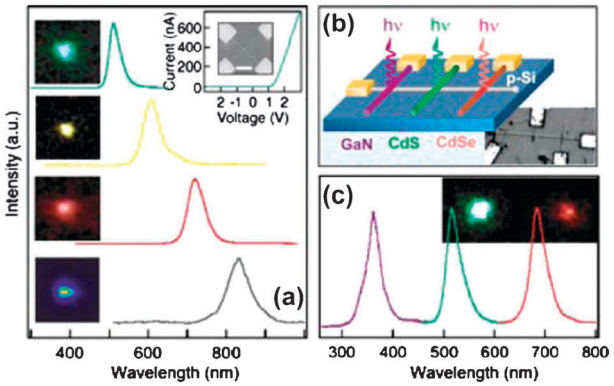

Fig. 24 (a) Electroluminescence (EL) spectra from crossed p–n diodes of p-Si and n-CdS, $CdS_{0.5}Se_{0.5}$, CdSe, and InP, respectively (top to bottom). Insets to the left are the corresponding electroluminescence images for CdS, $CdS_{1-x}Se_x$, CdSe, and InP nano-LEDs. The inset top-right shows representative current–voltage and SEM data recorded for a p-Si–n-CdS crossed nanowire junction (scale bar 1 μm). (b) Schematic and corresponding SEM image of a tricolor nano-LED array. (c) Normalized electroluminescence spectra and color images from the three elements (reprinted from ref. 179 Copyright 2005, with permission from WILEY-VCH Verlag GmbH & Co. KGaA).

4.5 Nanobioelectronic interfaces

In addition to gas and optical sensors, the applications of semiconductor nanowire field-effect transistors (FETs) in ultrasensitive biological sensors and cellular interfaces have been reported extensively in the last decade, especially by Lieber's group.[181–197] The principle of biological detection based on nanowire FETs is very simple. For example, when a single virus particle binds to an antibody receptor linked to the surface of a nanowire FET detector, it yields a conductance change due to the change in nanowire surface charge; when the virus particle subsequently unbinds, the conductance returns to the baseline. Through antibody-modified nanowire FETs, the limit of biological detection – single particle sensitivity (on the order of 50 viruses per μL or 80×10^{-18} M for viruses,[182] and 75 fg mL^{-1} or 2×10^{-15} M for cancer detection markers, prostate-specific antigen[183]) has been achieved. Particularly, the nanowire FETs can be assembled on either planar inorganic or biocompatible flexible plastic surfaces. And these nanowire device arrays can be implemented as a broad platform to measure/record electrical signals from individual neurons, cardiomyocytes, and heart tissue.[186,190,191] The reported signals are in millivolts range, which are considerably larger than those measured using planar, lithographically patterned devices, possibly due to enhanced coupling between the nanoscale device and cell membrane. Furthermore, high-density arrays of nanowire FETs can be used to map signals with high spatial resolution at the subcellular level.[190–194] These advances may have broad applications in fundamental biophysical studies of cellular function, drug assays and prosthetic devices.

4.6 Nano-resonators

Nanoelectromechanical resonators are very attractive for a new class of ultrafast, ultrasensitive devices,[10,172,198,199] Melosh *et al.*[172] reported a high-frequency nanomechanical resonator, which was fabricated by a technique named superlattice nanowire pattern transfer. The resonator contains nine Pt nanowires with 20 nm in diameter and 150 nm in pitch, suspended over a 0.75 μm trench on a bare Si wafer. The resonance frequency of this nano-resonator was measured to be ~162.5 MHz at 4 K using a magnetomotive technique. Particularly, Li *et al.*[10] demonstrated an interesting bottom-up assembly method to integrate large-area Si and Rh nanowire arrays each having over 2000 single-nanowire resonators on a Si chip. The integrated Si and Rh nanowire resonators had uniform and reproducible metal clamps. It was found that the resonators operated in the linear regime, namely, the resonance frequency was linear to geometric ratio D/L^2, where D and L are the nanowire diameter and length. The determined vacuum Q-factors for the Si and Rh nanowire resonators were ~4500 and ~1150, respectively.[10] These results indicate that nanowire resonators are promising candidates for highly sensitive resonance-based detection schemes.

5. Summary and outlook

In this paper, the recent advances in technologies developed for the integration of nanowire devices have been reviewed. Generally, one strategy is assembly of pre-grown nanowires/fibers on the desired substrate with alignment, including flow-assisted alignment, Langmuir–Blodgett technique, electric or magnetic-field-directed assembly, bubble-blown technique, and contact/roll printing techniques; the other one is direct growth of nanowires/fibers on the desired substrate or locations such as direct growth of vertical nanowire arrays, planar growth of nanowires, bridging method, and electrospinning.

Each assembly technique has its advantages and weaknesses. For instance, although microprobe manipulation and optical trapping can manipulate and deposit nanowires precisely, it seems a bit difficult to assemble nanowires on large scales at the present stage. Another example is that the direct growth of nanowires into devices on desired locations or substrates can reduce or eliminate post-processing of the nanowires and keep the wire surface clean. Understanding this point can help us select the right method for a specific device application. In some cases, as illustrated in Fig. 9c, appropriate combinations of two or more assembly techniques will be useful to improve the integration effect with fewer defects. Furthermore, there are still some challenges for efficient assembly of nanowires and nanofibers, especially for flexible/soft high-aspect ratio wires/fibers. One possible way is fixing one end of the nanowire/fiber while applying a shear force (*e.g.* fluid or gas flow) across the tangled structure.[33] Another possible way is direct growth and assembly of the flexible long nanowires/fibers *via* electrospinning, which seems to be the only method that can fabricate one-by-one continuous nanofibers of a variety of polymeric and ceramic materials on a large scale.

The "bottom-up" assembly of nanowires complements other "top-down" microfabrication techniques. By combining the current lithography technologies with the large-scale nanowire assembly techniques, a wide range of nanoscale electronics, sensors, bioelectronic interfaces, nanoresonators, nanogenerators, nanophotonics, and optoelectronics devices and circuits (*e.g.* programmable nanowire circuits for nanoprocessors[200])

from nanowire building blocks have been demonstrated. These encouraging achievements have shown the promising potential and practical approaches to realize nanowire based large-scale high performance devices, particularly in the area of flexible nanodevices.

Acknowledgements

This work was supported by the National Natural Science Foundation of China (Grant No.: 11074138 and 50825206), Shandong Province Natural Science Foundation for Distinguished Young Scholars (Grant No.: JQ201103), Taishan Scholars Program of Shandong Province, National Key Basic Research Development Program of China (973 special preliminary study plan) (Grant No. 2012CB722705), and the HKUST (Grant No.: DAG.09/10.EG09 and RPC11EG38).

References

1 Y. N. Xia, P. D. Yang, Y. G. Sun, Y. Y. Wu, B. Mayers, B. Gates, Y. D. Yin, F. Kim and H. Q. Yan, *Adv. Mater.*, 2003, **15**(5), 353.
2 S. Barth, F. Hernandez-Ramirez and J. D. Holmes, *Prog. Mater. Sci.*, 2010, **55**(6), 563.
3 S. V. N. T. Kuchibhatle, A. S. Karakoti, D. Bera and S. Seal, *Prog. Mater. Sci.*, 2007, **52**(5), 699.
4 Y. Z. Long, M. M. Li, C. Z. Gu, M. X. Wan, J. L. Duvail, Z. W. Liu and Z. Y. Fan, *Prog. Polym. Sci.*, 2011, **36**(10), 1415.
5 P. Xu, K. Xia, C. Z. Gu, L. Tang, H. F. Yang and J. J. Li, *Nat. Nanotechnol.*, 2008, **3**(2), 97.
6 A. Bachtold, P. Hadley, T. Nakanishi and C. Dekker, *Science*, 2001, **294**(5545), 317.
7 Y. Huang, X. F. Duan, Y. Cui, L. J. Lauhon, K. H. Kim and C. M. Lieber, *Science*, 2001, **294**(5545), 1313.
8 X. F. Duan, Y. Huang, Y. Cui, J. F. Wang and C. M. Lieber, *Nature*, 2001, **409**(6816), 6.
9 X. F. Duan, C. M. Niu, V. Sahi, J. Chen, J. W. Parce, S. Empedocles and J. L. Goldman, *Nature*, 2003, **425**(6955), 74.
10 M. W. Li, R. B. Bhiladvala, T. J. Morrow, J. A. Sioss, K. K. Lew, J. M. Redwing, C. D. Keating and T. S. Mayer, *Nat. Nanotechnol.*, 2008, **3**(2), 88.
11 K. Takei, T. Takahashi, J. C. Ho, H. Ko, A. G. Gillies, P. W. Leu, R. S. Fearing and A. Javey, *Nat. Mater.*, 2010, **9**(10), 821.
12 Z. L. Wang, *Nano Today*, 2010, **5**(6), 540.
13 T. Takahashi, K. Takei, E. Adabi, Z. Y. Fan, A. M. Niknejad and A. Javey, *ACS Nano*, 2010, **4**(10), 5855.
14 Z. Y. Fan, J. C. Ho, T. Takahashi, R. Yerushalmi, K. Takei, A. C. Ford, Y. L. Chueh and A. Javey, *Adv. Mater.*, 2009, **21**(37), 3730.
15 M. C. P. Wang and B. D. Gates, *Mater. Today*, 2009, **12**(5), 34.
16 Y. B. Li and J. J. Delaunay, *Progress toward nanowire device assembly technology*, in *Nanowires*, ed. P. Prete, INTECH, Croatia, 2010, ch. 19, pp. 373–394.
17 G. H. Yu and C. M. Lieber, *Pure Appl. Chem.*, 2010, **82**(12), 2295.
18 S. G. Rao, L. Huang, W. Setyawan and S. Hong, *Nature*, 2003, **425**(6953), 36.
19 J. B. Hannon, A. Afzali, C. Klinke and P. Avouris, *Langmuir*, 2005, **21**(19), 8569.
20 M. Lee, J. Im, B. Y. Lee, S. Myung, J. Kang, L. Huang, Y. K. Kwon and S. Hong, *Nat. Nanotechnol.*, 2006, **1**(1), 66.
21 J. Im, M. Lee, S. Myung, L. Huang, S. G. Rao, D. J. Lee, J. Koh and S. Hong, *Nanotechnology*, 2006, **17**(14), 3569.
22 S. Myung, M. Lee, G. T. Kim, J. S. Ha and S. Hong, *Adv. Mater.*, 2005, **17**(19), 2361.
23 J. Kang, S. Myung, B. Kim, D. Oh, G. T. Kim and S. Hong, *Nanotechnology*, 2008, **19**(9), 095303.
24 A. K. Salem, J. Chao, K. W. Leong and P. C. Searson, *Adv. Mater.*, 2004, **16**(3), 268.
25 M. Chen and P. C. Searson, *Adv. Mater.*, 2005, **17**(22), 2765.
26 J. Lee, A. A. Wang, Y. Rheem, B. Yoo, A. Mulchandani, W. Chen and N. V. Myung, *Electroanalysis*, 2007, **19**(22), 2287.
27 Y. Huang, X. F. Duan, Q. Wei and C. M. Lieber, *Science*, 2001, **291**(5504), 630.
28 Z. Y. Fan, J. C. Ho, Z. A. Jacobson, R. Yerushalmi, R. L. Alley, H. Razavi and A. Javey, *Nano Lett.*, 2008, **8**(1), 20.
29 Q. X. Tang, Y. H. Tong, W. P. Hu, Q. Wan and T. Bjfrnholm, *Adv. Mater.*, 2009, **21**(42), 4234.
30 R. Agarwal, K. Ladavac, Y. Roichman, G. H. Yu, C. M. Lieber and D. G. Grier, *Opt. Express*, 2005, **13**(22), 8906.
31 P. J. Pauzauskie, A. Radenovic, E. Trepagnier, H. Shroff, P. D. Yang and A. J. Liphardt, *Nat. Mater.*, 2006, **5**(2), 97.
32 Y. Huang and C. M. Lieber, *Pure Appl. Chem.*, 2004, **76**(12), 2051.
33 D. W. Wang, R. Tu, L. Zhang and H. J. Dai, *Angew. Chem., Int. Ed.*, 2005, **44**(19), 2925.
34 X. G. Xiong, L. Jaberansari, M. G. Hahm, A. Busnaina and Y. J. Jung, *Small*, 2007, **3**(12), 2006.
35 S. C. Yan, L. X. Lu, H. Meng, N. P. Huang and Z. D. Xiao, *Nanotechnology*, 2010, **21**(09), 095303.
36 Q. J. Guo, X. W. Teng, S. Rahman and H. Yang, *J. Am. Chem. Soc.*, 2003, **125**(3), 630.
37 L. J. Cote, F. Kim and J. X. Huang, *J. Am. Chem. Soc.*, 2009, **131**(3), 1043.
38 S. Acharya, J. P. Hill and K. Ariga, *Adv. Mater.*, 2009, **21**(29), 2959.
39 D. Whang, S. Jin, Y. Wu and C. M. Lieber, *Nano Lett.*, 2003, **3**(9), 1255.
40 A. Tao, F. Kim, C. Hess, J. Goldberger, R. R. He, Y. G. Sun, Y. N. Xia and P. D. Yang, *Nano Lett.*, 2003, **3**(9), 1229.
41 D. W. Wang, Y. L. Chang, Z. Liu and H. J. Dai, *J. Am. Chem. Soc.*, 2005, **127**(33), 11871.
42 S. Acharya, A. B. Panda, N. Belman, S. Efrima and Y. Golan, *Adv. Mater.*, 2006, **18**(2), 210.
43 J. Park, G. Shin and J. S. Ha, *Nanotechnology*, 2008, **19**(39), 395303.
44 L. Q. Mai, Y. H. Gu, C. H. Han, B. Hu, W. Chen, P. C. Zhang, L. Xu, W. L. Guo and Y. Dai, *Nano Lett.*, 2009, **9**(2), 826.
45 I. Patla, S. Acharya, L. Zeiri, J. Israelachvili, S. Efrima and Y. Golan, *Nano Lett.*, 2007, **7**(6), 1459.
46 F. Kim, S. Kwan, J. Akana and P. D. Yang, *J. Am. Chem. Soc.*, 2001, **123**(18), 4360.
47 X. L. Li, L. Zhang, X. R. Wang, I. Shimoyama, X. M. Sun, W. S. Seo and H. J. Dai, *J. Am. Chem. Soc.*, 2007, **129**(16), 4890.
48 J. W. Liu, J. H. Zhu, C. L. Zhang, H. W. Liang and S. H. Yu, *J. Am. Chem. Soc.*, 2010, **132**(26), 8945.
49 S. Jin, D. Whang, M. C. McAlpine, R. S. Friedman, Y. Wu and C. M. Lieber, *Nano Lett.*, 2004, **4**(5), 915.
50 G. H. Yu, A. Y. Cao and C. M. Lieber, *Nat. Nanotechnol.*, 2007, **2**(6), 372.
51 A. Javey, S. M. Nam, R. S. Friedman, H. Yan and C. M. Lieber, *Nano Lett.*, 2007, **7**(3), 773.
52 Z. Y. Fan, J. C. Ho, Z. A. Jacobson, R. Yerushalmi, R. L. Alley, H. Razavi and A. Javey, *Nano Lett.*, 2008, **8**(1), 20.
53 G. Zhu, R. S. Yang, S. H. Wang and Z. L. Wang, *Nano Lett.*, 2010, **10**(8), 3151.
54 R. Yerushalmi, Z. A. Jacobson, J. C. Ho, Z. Y. Fan and A. Javey, *Appl. Phys. Lett.*, 2007, **91**(20), 203104.
55 Y. K. Chang and F. C. N. Hong, *Nanotechnology*, 2009, **20**(19), 195302.
56 L. Y. Wen, K. M. Wong, Y. G. Fang, M. H. Wu and Y. Lei, *J. Mater. Chem.*, 2011, **21**(20), 7090.
57 Y. K. Kim, P. S. Kang, D. I. Kim, G. Shin, G. T. Kim and J. S. Ha, *Small*, 2009, **5**(6), 727.
58 Y. Z. Long, J. Zheng, B. Sun and Z. H. Zhang, *China patent*, No. 201110255577.3, 2011.
59 B. D. Gates, *Nat. Nanotechnol.*, 2010, **5**(7), 484.
60 P. A. Smith, C. D. Nordquist, T. N. Jackson, T. S. Mayer, B. R. Martin, J. Mbindyo and T. E. Mallouk, *Appl. Phys. Lett.*, 2000, **77**(9), 1399.
61 Y. L. Liu, J. H. Chung, W. K. Liu and R. S. Ruoff, *J. Phys. Chem. B*, 2006, **110**(29), 14098.
62 D. Q. Wang, R. Zhu, Z. Y. Zhou and X. Y. Ye, *Appl. Phys. Lett.*, 2007, **90**(10), 103110.
63 R. H. Zhou, H. C. Chang, V. Protasenko, M. Kuno, A. K. Singh, D. Jena and H. Xing, *J. Appl. Phys.*, 2007, **101**(7), 073704.

64 Y. K. Chang and F. C. N. Hong, *Nanotechnology*, 2009, **20**(23), 235202.
65 M. C. P. Wang, X. Zhang, E. Majidi, K. Nedelec and B. D. Gates, *ACS Nano*, 2010, **4**(5), 2607.
66 E. M. Freer, O. Grachev, X. F. Duan, S. Martin and D. P. Stumbo, *Nat. Nanotechnol.*, 2010, **5**(7), 525.
67 C. H. Lee, D. R. Kim and X. L. Zheng, *Nano Lett.*, 2010, **10**(12), 5116.
68 A. O'Riordan, D. Iacopino, P. Lovera, L. Floyd, K. Reynolds and G. Redmond, *Nanotechnology*, 2011, **22**(10), 105602.
69 S. J. Papadakis, J. A. Hoffmann, D. Deglau, A. Chen, P. Tyagi and D. H. Gracias, *Nanoscale*, 2011, **3**(3), 1059.
70 M. Liu, J. Lagdani, H. Imrane, C. Pettiford, J. Lou, S. Yoon, V. G. Harris, C. Vittoria and N. X. Sun, *Appl. Phys. Lett.*, 2007, **90**(10), 103105.
71 C. M. Hangarter, Y. Rheem, B. Yoo, E. H. Yang and N. V. Myung, *Nanotechnology*, 2007, **18**(20), 205303.
72 C. M. Hangarter and N. V. Myung, *Chem. Mater.*, 2005, **17**(6), 1320.
73 M. A. Bangar, C. M. Hangarter, B. Yoo, Y. Rheem, W. Chen, A. Mulchandani and N. V. Myung, *Electroanalysis*, 2009, **21**(1), 61.
74 B. Yoo, Y. Rheem, W. P. Beyermann and N. V. Myung, *Nanotechnology*, 2006, **17**(10), 2512.
75 M. Tanase, E. J. Felton, D. S. Gray, A. Hultgren, C. S. Chen and D. H. Reich, *Lab Chip*, 2005, **5**(6), 598.
76 P. D. Yang, H. Q. Yan, S. Mao, R. Russo, J. Johnson, R. Saykally, N. Morris, J. Pham, R. R. He and H. J. Choi, *Adv. Funct. Mater.*, 2002, **12**(5), 323.
77 H. J. Fan, W. Lee, R. Scholz, A. Dadgar, A. Krost, K. Nielsch and M. Zacharias, *Nanotechnology*, 2005, **16**(6), 913.
78 H. J. Zhou, J. Fallert, J. Sartor, R. J. B. Dietz, C. Klingshirn, H. Kalt, D. Weissenberger, D. Gerthsen, H. B. Zeng and W. P. Cai, *Appl. Phys. Lett.*, 2008, **92**(13), 132112.
79 Y. G. Wei, W. Z. Wu, R. Guo, D. J. Yuan, S. Das and Z. L. Wang, *Nano Lett.*, 2010, **10**(9), 3414.
80 S. Zhang, Y. Shen, H. Fang, S. Xu, J. H. Song and Z. L. Wang, *J. Mater. Chem.*, 2010, **20**(47), 10606.
81 D. Gao, R. R. He, C. Carraro, R. T. Howe, P. D. Yang and R. Maboudian, *J. Am. Chem. Soc.*, 2005, **127**(13), 4574.
82 P. Manandhar, E. A. Akhadov, C. Tracy and S. T. Picraux, *Nano Lett.*, 2010, **10**(6), 2126.
83 J. M. Weisse, D. R. Kim, C. H. Lee and X. L. Zheng, *Nano Lett.*, 2011, **11**(3), 1300.
84 J. J. Chao, D. S. Wang, S. C. Shiu, S. C. Hung and C. F. Lin, *Semicond. Sci. Technol.*, 2010, **25**(6), 065014.
85 H. Fang, D. J. Yuan, R. Guo, S. Zhang, R. P. S. Han, S. Das and Z. L. Wang, *ACS Nano*, 2011, **5**(2), 1476.
86 C. Wongchoosuk, K. Subannajui, A. Menzel, I. A. Burshtein, S. Tamir, Y. Lifshitz and M. Zacharias, *J. Phys. Chem. C*, 2011, **115**(3), 757.
87 G. H. Lee, Y. S. Woo, J. E. Yang, D. H. Lee, C. J. Kim and M. H. Jo, *Angew. Chem., Int. Ed.*, 2009, **48**(40), 7366.
88 Z. L. Wang, R. Yang, J. Zhou, Y. Qin, C. Xu, Y. F. Hu and S. Xu, *Mater. Sci. Eng., R*, 2010, **70**(3–6), 320.
89 B. Nikoobakht, *Chem. Mater.*, 2007, **19**(22), 5279.
90 S. A. Fortuna, J. G. Wen, I. S. Chun and X. L. Li, *Nano Lett.*, 2008, **8**(12), 4421.
91 S. A. Fortuna and X. L. Li, *IEEE Electron Device Lett.*, 2009, **30**(6), 593.
92 G. Q. Zhang, K. Tateno, H. Gotoh and H. Nakano, *Nanotechnology*, 2010, **21**(9), 095607.
93 G. Q. Zhang, K. Tateno, H. Gotoh and T. Sogawa, *Appl. Phys. Express*, 2010, **3**(10), 105002.
94 Z. Zhang, L. M. Wong, H. X. Wang, Z. P. Wei, W. Zhou, S. J. Wang and T. Wu, *Adv. Funct. Mater.*, 2010, **20**(15), 2511.
95 Y. Liang, H. Y. Xu and S. K. Hark, *J. Phys. Chem. C*, 2010, **114**(18), 8343.
96 K. Haraguchi, K. Hiruma, T. Katsuyama, K. Tominaga, M. Shirai and T. Shimada, *Appl. Phys. Lett.*, 1996, **69**(3), 386.
97 M. S. Islam, S. Sharma, T. I. Kamins and R. S. Williams, *Nanotechnology*, 2004, **15**(5), L5.
98 M. Tabib-Azar, M. Nassirou, R. Wang, S. Sharma, T. I. Kamins, M. S. Islam and R. S. Williams, *Appl. Phys. Lett.*, 2005, **87**(11), 113102.
99 R. R. He and P. D. Yang, *Nat. Nanotechnol.*, 2006, **1**(1), 42.
100 R. S. Chen, S. W. Wang, Z. H. Lan, J. T. H. Tsai, C. T. Wu, L. C. Chen, K. H. Chen, Y. S. Huang and C. C. Chen, *Small*, 2008, **4**(7), 925.
101 J. S. Lee, M. S. Islam and S. Kim, *Sens. Actuators, B*, 2007, **126**(1), 73.
102 Y. Qin, R. S. Yang and Z. L. Wang, *J. Phys. Chem. C*, 2008, **112**(48), 18734.
103 Y. B. Li, A. Paulsen, I. Yamada, Y. Koide and J. J. Delaunay, *Nanotechnology*, 2010, **21**(29), 295502.
104 N. P. Kobayashi, S. Mathai, X. M. Li, V. J. Logeeswaran, M. S. Islam, A. Lohn, T. Onishi, J. Straznicky, S. Y. Wang and R. S. Williams, *Appl. Phys. A: Mater. Sci. Process.*, 2009, **95**(4), 1005.
105 Y. B. Li, T. Tokizono, M. Y. Liao, M. Zhong, Y. Koide, I. Yamada and J. J. Delaunay, *Adv. Funct. Mater.*, 2010, **20**(22), 3972.
106 N. J. Quitoriano and T. I. Kamins, *Nanotechnology*, 2011, **22**(6), 065201.
107 D. R. Kim, C. H. Lee and X. L. Zheng, *Nano Lett.*, 2010, **10**(3), 1050.
108 D. H. Reneker and A. L. Yarin, *Polymer*, 2008, **49**(10), 2387.
109 Z. M. Huang, Y. Z. Zhang, M. Kotaki and S. Ramakrishna, *Compos. Sci. Technol.*, 2003, **63**(15), 2223.
110 M. M. Li, D. Y. Yang, Y. Z. Long and H. W. Ma, *Nanoscale*, 2010, **2**(2), 218.
111 C. C. Tang, J. C. Chen, Y. Z. Long, H. X. Yin, B. Sun and H. D. Zhang, *Chin. Phys. Lett.*, 2011, **28**(5), 056801.
112 B. Sun, Y. Z. Long, F. Yu, M. M. Li, H. D. Zhang, W. J. Li and T. X. Xu, *Nanoscale*, 2012, **4**(6), 2134.
113 J. S. Tan, Y. Z. Long and M. M. Li, *Chin. Phys. Lett.*, 2008, **25**(8), 3067.
114 C. L. Shao, H. Kim, J. Gong and D. Lee, *Nanotechnology*, 2002, **13**(5), 635.
115 D. Li and Y. N. Xia, *Adv. Mater.*, 2004, **16**(14), 1151.
116 H. D. Zhang, Y. Z. Long, Z. J. Li, B. Sun and C. H. Sheng, *Adv. Mater. Res.*, 2012, **418–420**, 684.
117 W. E. Teo and S. Ramakrishna, *Nanotechnology*, 2006, **17**(14), R89.
118 B. Sundaray, V. Subramanian, T. S. Natarajan, R. Z. Xiang, C. C. Chang and W. S. Fann, *Appl. Phys. Lett.*, 2004, **84**(7), 1222.
119 H. Pan, L. M. Li, L. Hu and X. J. Cui, *Polymer*, 2006, **47**(14), 4901.
120 P. Katta, M. Alessandro, R. D. Ramsier and G. G. Chase, *Nano Lett.*, 2004, **4**(11), 2215.
121 A. Theron, E. Zussman and A. L. Yarin, *Nanotechnology*, 2001, **12**(3), 384.
122 E. Zussman, A. Theron and A. L. Yarin, *Appl. Phys. Lett.*, 2003, **82**(6), 973.
123 Y. Z. Long and M. M. Li, *A modified electrospinning setup for preparation of aligned, twisted polymer nanofibers*, *China patent*, No. ZL200820232745.0, 2008.
124 H. S. Shim, S. I. Na, S. H. Nam, H. J. Ahn, H. J. Kim, D. Y. Kim and W. B. Kim, *Appl. Phys. Lett.*, 2008, **92**(18), 183107.
125 S. J. Wu, Q. D. Tai and F. Yan, *J. Phys. Chem. C*, 2010, **114**(13), 6197.
126 Q. D. Tai, X. Z. Zhao and F. Yan, *J. Mater. Chem.*, 2010, **20**(35), 7366.
127 D. Li, Y. L. Wang and Y. N. Xia, *Nano Lett.*, 2003, **3**(8), 1167–1171.
128 H. Yan, L. Q. Liu and Z. Zhang, *Appl. Phys. Lett.*, 2009, **95**(14), 143114.
129 M. Pokorny, K. Niedoba and V. Velebny, *Appl. Phys. Lett.*, 2010, **96**(19), 193111.
130 Q. H. Zhang, Z. J. Chang, M. F. Zhu, X. M. Mo and D. J. Chen, *Nanotechnology*, 2007, **18**(11), 115611.
131 Z. T. Zhu, L. F. Zhang, J. Y. Howe, Y. L. Liao, J. T. Speidel, S. Smith and H. Fong, *Chem. Commun.*, 2009, 2568.
132 D. D. Lin, H. Wu, X. L. Qin and W. Pan, *Appl. Phys. Lett.*, 2009, **95**(11), 112104.
133 J. T. McCann, J. I. L. Chen, D. Li, Z. G. Ye and Y. N. Xia, *Chem. Phys. Lett.*, 2006, **424**(1–3), 162.
134 H. W. Lu, W. Zeng, Y. S. Li and Z. W. Fu, *J. Power Sources*, 2007, **164**(2), 874.
135 Y. J. Qiu, J. Yu, J. Rafique, J. Yin, X. D. Bai and E. G. Wang, *J. Phys. Chem. C*, 2009, **113**(26), 1228.

136 D. Li, T. Herricks and Y. N. Xia, *Appl. Phys. Lett*., 2003, **83**(22), 4586.
137 H. Wu, R. Zhang, X. X. Liu, D. D. Lin and W. Pan, *Chem. Mater*., 2007, **19**(14), 3506.
138 D. Li and Y. N. Xia, *Nano Lett*., 2004, **4**(5), 933.
139 S. H. Choi, G. Ankonina, D. Y. Youn, S. G. Oh, J. M. Hong, A. Rothschild and I. D. Kim, *ACS Nano*, 2009, **3**(9), 2623.
140 M. Zhou, J. Y. Zhou, R. S. Li and E. Q. Xie, *Nanoscale Res. Lett*., 2010, **5**(2), 279.
141 Y. Liu, C. Gao, X. Pan, X. An, Y. Xie, M. Zhou, J. Song, H. Zhang, Z. Liu, Q. Zhao, Y. Zhang and E. Xie, *Appl. Surf. Sci*., 2011, **257**(6), 2264.
142 J. M. Deitzel, J. D. Kleinmeyer, J. K. Hirvonen and N. C. B. Tan, *Polymer*, 2001, **42**(19), 8163.
143 L. S. Carnell, E. J. Siochi, N. M. Holloway, R. M. Stephens, C. Rhim, L. E. Niklason and R. L. Clark, *Macromolecules*, 2008, **41**(14), 5345.
144 X. J. Cui, L. M. Li and F. Xu, *Appl. Phys. A*, 2011, **103**(1), 167.
145 B. K. Gu, K. Sohn, S. J. Kim and S. I. Kim, *J. Nanosci. Nanotechnol*., 2007, **7**(11), 4202.
146 Y. Q. Wu, L. A. Carnell and R. L. Clark, *Polymer*, 2007, **48**(19), 5653.
147 D. Y. Yang, B. Lu, Y. Zhao and X. Y. Jiang, *Adv. Mater*., 2007, **19**(21), 3702.
148 J. A. Ajao, A. A. Abiona, S. Chigome, A. Y. Fasasi, G. A. Osinkolu and M. Maaza, *J. Mater. Sci*., 2010, **45**(9), 2324.
149 Y. Q. Liu, X. P. Zhang, Y. N. Xia and H. Yang, *Adv. Mater*., 2010, **22**(22), 2454.
150 E. P. S. Tan, S. Y. Ng and C. T. Lim, *Biomaterials*, 2005, **26**(13), 1453.
151 Y. Z. Long, J. Zheng, F. Shao, W. H. Han, H. X. Yin and Z. H. Zhang, *An electrospinning setup with a modified double-frame collector for fabrication of helical twisted nanofibers*, *China patent*, No. 201110137420.0, 2011.
152 M. M. Li, Y. Z. Long, D. Y. Yang, J. S. Sun, H. X. Yin, Z. L. Zhao, W. H. Kong, X. Y. Jiang and Z. Y. Fan, *J. Mater. Chem*., 2011, **21**, 13159.
153 M. R. Badrossamay, H. A. McIlwee, G. A. Goss and K. K. Parker, *Nano Lett*., 2010, **10**(6), 2257.
154 C. C. Liao, S. S. Hou, C. C. Wang and C. Y. Chen, *Polymer*, 2010, **51**(13), 2887.
155 M. Khamforoush and M. Mahjob, *Mater. Lett*., 2011, **65**(3), 453.
156 D. H. Sun, C. Chang, S. Li and L. W. Lin, *Nano Lett*., 2006, **6**(4), 839.
157 G. S. Bisht, G. Canton, A. Mirsepassi, L. Kulinsky, S. Oh, D. Dunn-Rankin and M. J. Madou, *Nano Lett*., 2011, **11**(4), 1831.
158 C. Chang, K. Limkrailassiri and L. W. Lin, *Appl. Phys. Lett*., 2008, **93**(12), 123111.
159 G. F. Zheng, W. W. Li, X. Wang, D. Z. Wu, D. H. Sun and L. W. Lin, *J. Phys. D: Appl. Phys*., 2010, **43**(41), 415501.
160 J. Pu, X. J. Yan, Y. D. Jiang, C. Chang and L. W. Lin, *Sens. Actuators, A*, 2010, **164**(1–2), 131.
161 C. Chang, V. H. Tran, J. B. Wang, Y. K. Fuh and L. W. Lin, *Nano Lett*., 2010, **10**(2), 726.
162 T. D. Brown, P. D. Dalton and D. W. Hutmacher, *Adv. Mater*., 2011, **23**(47), 5651.
163 M. Rinaldi, F. Ruggieri, L. Lozzi and S. Santucci, *J. Vac. Sci. Technol., B*, 2009, **27**(4), 1829.
164 D. M. Zhang and J. Chang, *Adv. Mater*., 2007, **19**(21), 3664.
165 D. M. Zhang and J. Chang, *Nano Lett*., 2008, **8**(10), 3283.
166 Z. W. Ding, A. Salim and B. Ziaie, *Langmuir*, 2009, **25**(17), 9648.
167 J. Rafique, J. Yu, J. L. Yu, G. Fang, K. W. Wong, Z. Zheng, H. C. Ong and W. M. Lau, *Appl. Phys. Lett*., 2007, **91**(6), 063126.
168 C. R. Martin, *Science*, 1994, **266**(5193), 1961.
169 J. L. Duvail, S. Dubois, S. Demoustier-Champagne, Y. Z. Long and L. Piraux, *Int. J. Nanotechnol*., 2008, **5**(6–8), 838.
170 Y. F. Li, J. H. Zhang and B. Yang, *Nano Today*, 2010, **5**(2), 117.
171 J. Zhu, Z. F. Yu, S. H. Fan and Y. Cui, *Mater. Sci. Eng., R*, 2010, **70**(3–6), 330.
172 N. A. Melosh, A. Boukai, F. Diana, B. Gerardot, A. Badolato, P. M. Petroff and J. R. Heath, *Science*, 2003, **300**(5616), 112.
173 K. Skucha, Z. Y. Fan, K. Jeon, A. Javey and B. Boser, *Sens. Actuators, B*, 2010, **145**(1), 232.
174 Z. Y. Fan, J. C. Ho, Z. A. Jacobson, H. Razavi and A. Javey, *Proc. Natl. Acad. Sci. U. S. A*., 2008, **105**(32), 11066.
175 M. Law, L. E. Greene, J. C. Johnson, R. Saykally and P. D. Yang, *Nat. Mater*., 2005, **4**(6), 455.
176 Z. Y. Fan, H. Razavi, J. W. Do, A. Moriwaki, O. Ergen, Y. L. Chueh, P. W. Leu, J. C. Ho, T. Takahashi, L. A. Reichertz, S. Neale, K. Yu, M. Wu, J. W. Ager and A. Javey, *Nat. Mater*., 2009, **8**(8), 648.
177 A. I. Hochbaum and P. D. Yang, *Chem. Rev*., 2010, **110**(1), 527.
178 K. Q. Peng and S. T. Lee, *Adv. Mater*., 2011, **23**(2), 198.
179 Y. Huang, X. F. Duan and C. M. Lieber, *Small*, 2005, **1**(1), 142.
180 M. C. McAlpine, R. S. Friedman, S. Jin, K. Lin, W. U. Wang and C. M. Lieber, *Nano Lett*., 2003, **3**(11), 1531.
181 Y. Cui, Q. Wei, H. Park and C. M. Lieber, *Science*, 2001, **293**(5533), 1289.
182 F. Patolsky, G. Zheng, O. Hayden, M. Lakadamyali, X. Zhuang and C. M. Lieber, *Proc. Natl. Acad. Sci. U. S. A*., 2004, **101**(39), 14017.
183 G. Zheng, F. Patolsky, Y. Cui, W. U. Wang and C. M. Lieber, *Nat. Biotechnol*., 2005, **23**(10), 1294.
184 P. Xie, Q. H. Xiong, Y. Fang, Q. Qing and C. M. Lieber, *Nat. Nanotechnol*., 2012, **7**(2), 119.
185 N. A. Kotov, J. O. Winter, I. P. Clements, E. Jan, B. P. Timko, S. Campidelli, S. Pathak, A. Mazzatenta, C. M. Lieber, M. Prato, R. V. Bellamkonda, G. A. Silva, N. W. S. Kam, F. Patolsky and L. Ballerini, *Adv. Mater*., 2009, **21**(40), 3970.
186 F. Patolsky, B. P. Timko, G. Yu, Y. Fang, A. B. Greytak, G. Zheng and C. M. Lieber, *Science*, 2006, **313**(5790), 100.
187 T. Cohen-Karni, Q. Qing, Q. Li, Y. Fang and C. M. Lieber, *Nano Lett*., 2010, **10**(3), 1098.
188 G. F. Zheng, X. P. A. Gao and C. M. Lieber, *Nano Lett*., 2010, **10**(8), 3179.
189 X. P. A. Gao, G. F. Zheng and C. M. Lieber, *Nano Lett*., 2010, **10**(2), 547.
190 B. P. Timko, T. Cohen-Karni, G. H. Yu, Q. Qing, B. Z. Tian and C. M. Lieber, *Nano Lett*., 2009, **9**(2), 914.
191 T. Cohen-Karni, B. P. Timko, L. E. Weiss and C. M. Lieber, *Proc. Natl. Acad. Sci. U. S. A*., 2009, **106**(18), 7309.
192 Q. Qing, S. K. Pal, B. Z. Tian, X. J. Duan, B. P. Timko, T. Cohen-Karni, V. N. Murthy and C. M. Lieber, *Proc. Natl. Acad. Sci. U. S. A*., 2010, **107**(5), 1882.
193 B. Z. Tian, T. Cohen-Karni, Q. Qing, X. J. Duan, P. Xie and C. M. Lieber, *Science*, 2010, **329**(5993), 830.
194 Z. Jiang, Q. Qing, P. Xie, R. X. Gao and C. M. Lieber, *Nano Lett*., 2012, **12**(3), 1711.
195 X. J. Duan, R. X. Gao, P. Xie, T. Cohen-Karni, Q. Qing, H. S. Choe, B. Z. Tian, X. C. Jiang and C. M. Lieber, *Nat. Nanotechnol*., 2012, **7**(3), 174.
196 B. P. Timko, T. Cohen-Karni, Q. Qing, B. Z. Tian and C. M. Lieber, *IEEE Trans. Nanotechnol*., 2010, **9**(3), 269.
197 B. Z. Tian and C. M. Lieber, *Pure Appl. Chem*., 2011, **83**(12), 2153.
198 V. Cimalla, F. Niebelschütz, K. Tonisch, C. Foerster, K. Brueckner, I. Cimalla, T. Friedrich, J. Pezoldt, R. Stephan, M. Hein and O. Ambacher, *Sens. Actuators, B*, 2007, **126**(1), 24.
199 T. Henry, K. Kim, Z. Y. Ren, C. Yerino, J. Han and H. X. Tang, *Nano Lett*., 2007, **7**(11), 3315.
200 H. Yan, H. S. Choe, S. W. Nam, Y. J. Hu, S. Das, J. F. Klemic, J. C. Ellenbogen and C. M. Lieber, *Nature*, 2011, **470**(7333), 240.